

Appendix A

Sea Level Calculations at Horns Rev

Observations from the off-shore tide gauge at Horns Rev (55°34.519' N; 07°26.140' E) have been obtained for the two periods:

1. period: August 26. 1997 - December 4. 1997
2. period: December 4. 1997 - April 29. 1998

At the instrument inspection and data collection at 4/12 1997 a new instrument was re-mounted at a slightly different position resulting in an off-set of approximately 0.5 m in the water depth, and the two data periods have been analyzed separately.

The instrument measures at the sea bed the total pressure caused by the weight of the overlaying water column plus the atmospheric pressure. By assuming hydrostatic pressure the relation between the observed bottom pressure and the sea level variations is given by:

$$p_{obs.} = p_{water} + p_{atm.} = -\rho_w(S, T, p) g z + p_{atm.}$$

where $z = -(H + \eta)$ is the negative water depth consisting of the height of the water column H at Mean Sea Level (MSL), and η the actual deviation from MSL. The bottom pressure instrument measures the temperature T [°C], the conductivity [10^{-3} ohm $^{-1}$ cm $^{-1}$] and the pressure [psi]. The conversion from the pressure unit psi (=lb/in 2) to the SI pressure unit Pa is:

$$1 \text{ psi} = 6.894757 \cdot 10^3 \text{ Pa} .$$

The total height of the water column, z is calculated by:

$$z = - \frac{6.894757 \cdot 10^3 \frac{\text{Pa}}{\text{psi}} (p_{obs.} - p_{atm})_{\text{psi}}}{\rho_w(T, S, p) g} ,$$

where g is the acceleration of gravity in m/s 2 , p and p_{atm} the total pressure and the atmospheric pressure, respectively, both measured in psi, and $\rho_w(T, S, p)$ the density of the water [kg/m 3] depending of the water temperature T [C°], salinity S [Practical Salinity Units (PSU)] and

pressure p [hPa]. The density of the water ρ_w is calculated as (*UNESCO*, 1981):

$$\begin{aligned} \rho_w = & 999.842594 + 6.793952 \cdot 10^{-2} T - 9.095290 \cdot 10^{-3} T^2 \\ & + 1.001685 \cdot 10^{-4} T^3 - 1.120083 \cdot 10^{-6} T^4 + 6.536332 \cdot 10^{-9} T^5 \\ & + S [0.824493 - 4.0899 \cdot 10^{-3} T + 7.6438 \cdot 10^{-5} T^2 - 8.2467 \cdot 10^{-7} T^3 + 5.3875 \cdot 10^{-9} T^4] \\ & + S^{1.5} [-5.72466 \cdot 10^{-3} + 1.0227 \cdot 10^{-4} T - 1.6546 \cdot 10^{-6} T^2] \\ & + S^2 \cdot 4.8314 \cdot 10^{-4}. \end{aligned}$$

In general the density of the water also depends on the pressure, but at 20 m depth the pressure only effects the density with less than 0.1 %, and the pressure dependency in the water density has been neglected.

The water temperature measured at the sea bed at approximately 22 m is used as representing the temperature in the whole water column. The conductivity sensor at the instrument failed during both data periods, and a constant value for the salinity of 34 PSU have been used for the sea level calculations. These uncertainties in the water salinity and temperature have introduced errors in the calculations of the sea level. An estimate of the size of the error can be obtained from statistical data from the Vyl light vessels that until 1970 did operate at the position (55°25' N, 6°34' E) approximately 20 km SSE of the location of the instrument at Horns Rev. The light vessel data show an annual variation in the salinity of approximately 3 PSU at the surface in the interval 31.0-34.0 PSU and at 20 m water depth a variation in the interval of 32.0-34.0 PSU (*Sparre*, 1984b). The temperature data show a depth variation of approximately 2 °C between surface and 20 m (*Sparre*, 1984a). The errors in the water depth calculation caused by these temperature and salinity variations may therefore be estimated to be of the order of a few cm.

The Influence from the Atmospheric Pressure

For calculation of the sea level the atmospheric pressure has been removed from the observations. The nearest observations of the atmospheric pressure are obtained from the meteorological station at Blåvands Huk (55°33' N; 08°05' E) operated by DMI. This synop station is located at the Danish North Sea coast 18 m above the sea surface and 42 km east of the off-shore instrument at Horns Rev. The atmospheric pressure observations are available at a sampling rate of 3 hours, and a cubic spline interpolation has been used to interpolate to hourly values. These atmospheric pressure observations have been used to remove the influence from the atmospheric load in the sea level calculations. The distance between the off-shore station at Horns Rev and the meteorological synop station may introduce an error in the calculated sea level. The magnitude of this error is highly dependent on the weather situation. A worst case pressure difference between the two stations is 5 hPa which may introduce an error in the sea level calculation of approximately 5 cm. For more calm weather situations the sea level error will be of the order of 1 cm. To estimate the influence from the distance between the off-shore observations and the coastal atmospheric observations, model simulated values for the atmospheric surface pressure from the High Resolution Limited Area Model (HIRLAM) have been included. A scatter plot of the Horns Rev water depth time series calculated with the atmospheric pressure from the observations from Blåvands Huk and the model simulated values is shown in Figure A.1. No

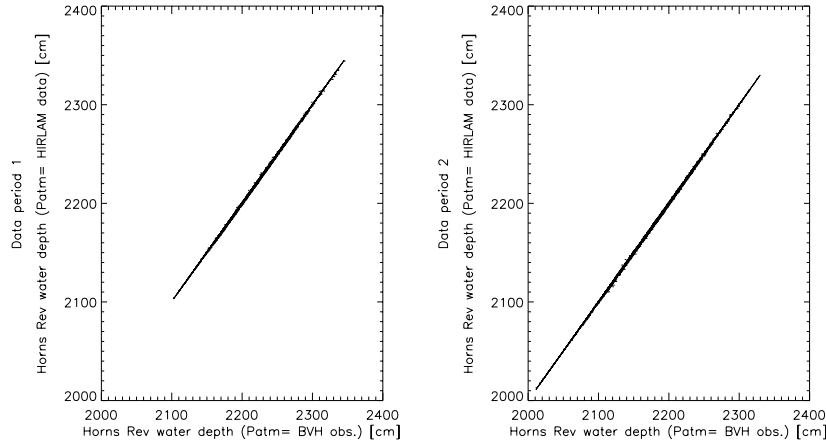


Figure A.1: Scatter plot between Horns Rev water depth calculations, where the atmospheric pressure has been removed with observations from the synop station at Blåvands Huk (BVH) and HIRLAM simulated values, respectively.

influence on the sea level calculations is found by using the HIRLAM data instead of the coastal observations for removal of the atmospheric load. A third water depth time series have been calculated by assuming a constant atmospheric pressure of 1013 hPa. This time series have been constructed to test the influence to the atmospheric pressure variations on the sea level and the ocean tides. The standard deviations for the calculated sea level time series are shown in Table A.1 for the three different time series with and without the atmospheric pressure variations removed. A larger variation in the sea level is seen for the time series where the atmospheric pressure variations have been removed.

Scatter plots of the calculated total water depth at Horns Rev for the three different atmospheric pressure calculations are seen in Figures A.2 and A.3 for the two data periods as function of sea levels from the coastal tide gauge station at Esbjerg 65 km E of Horns Rev. A linear correlation coefficient has been estimated to be in the interval $r=0.88-0.91$, with the lowest correlation for the Horns Rev data where the atmospheric pressure variations have not been removed. The inclination of the linear fit shows the shoaling effect on a factor of approximately 2 in the sea level variations from Horns Rev towards the coast.

Data period:	St. dev. ($p_{atm.}=1013$ hPa)	St. dev. ($p_{atm.}=obs.$)	St. dev. ($p_{atm.}=model$)
1	35.1 cm	38.1 cm	38.0 cm
2	38.5 cm	42.5 cm	42.5 cm

Table A.1: The standard deviations for the sea level time series calculated without the atmospheric pressure variations removed ($p_{atm.} = 0$) and with the atmospheric pressure variations removed by using observations and model simulations.

Sea level residuals from Horns Rev for the two time series calculated with constant and observed atmospheric pressure are shown in Figure A.4 together with the corresponding residuals from the Esbjerg tide gauge station. A larger correlation between the residuals at Horns Rev and Esbjerg is seen for the Horns Rev data where the atmospheric pressure variations have been removed from the observed sea level variability.

An estimation of the IB effect (see Section 5.2.1) for the Horns Rev data is shown in Figure A.5 as function of the atmospheric pressure observations from Blåvands Huk. The IB effect is estimated for the Horns Rev data set calculated with the atmospheric pressure contribution represented as the constant values of 1013 hPa, and with the observations obtained from the synop station at Blåvands Huk, respectively. A significant different residual pattern is observed for the two data periods, and for the two calculated sea level records, with the IB effect estimated in the range from no effect to -1.3 cm/hPa. For the Horns Rev sea level residuals where the atmospheric pressure variability has been removed, the IB effects are estimated to be -0.6 cm/hPa and -1.3 cm/hPa for the two data sampling periods, respectively.

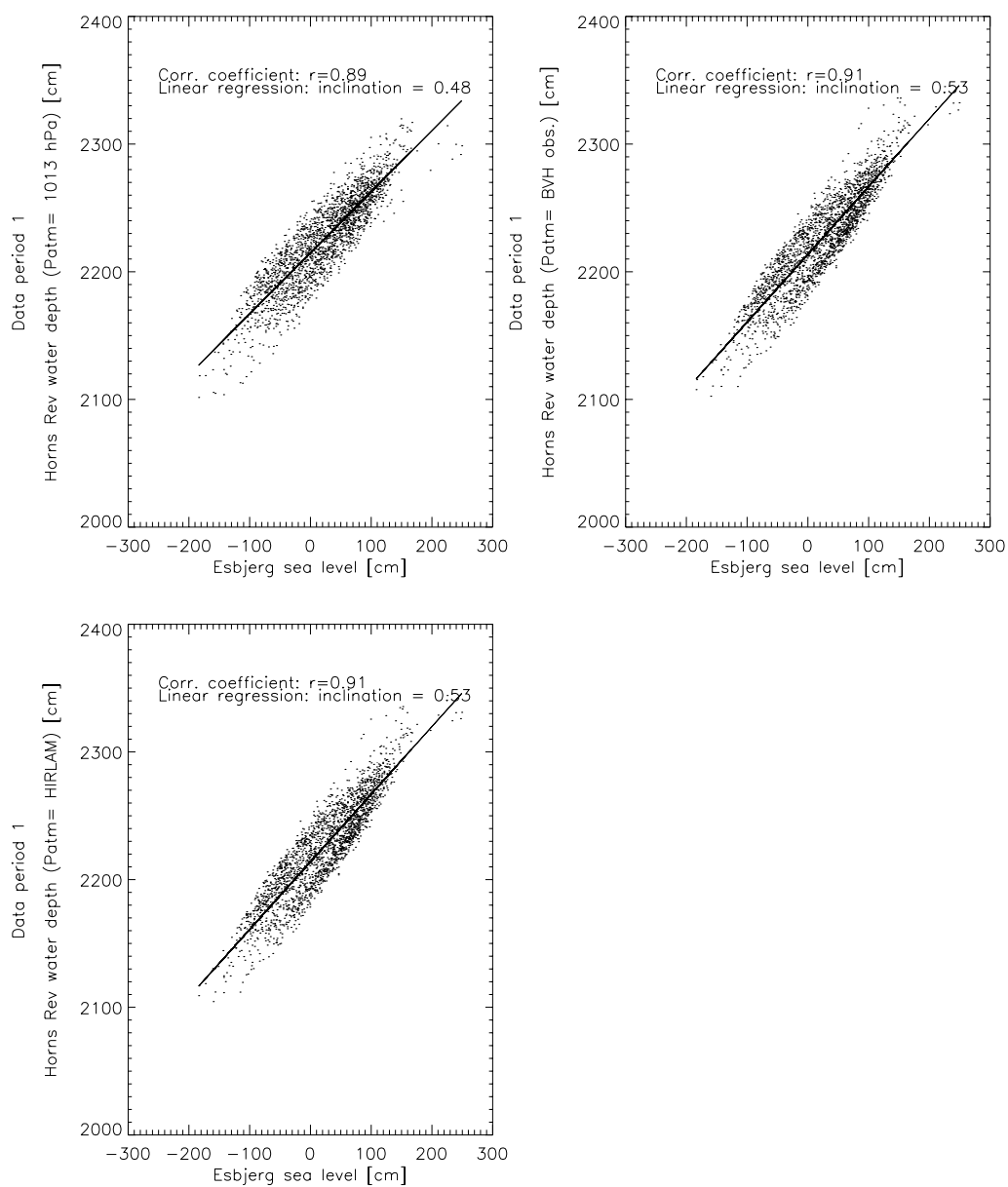


Figure A.2: Scatter plot between Horns Rev water depths and corresponding sea level data from Esbjerg. Shown for data period 1.

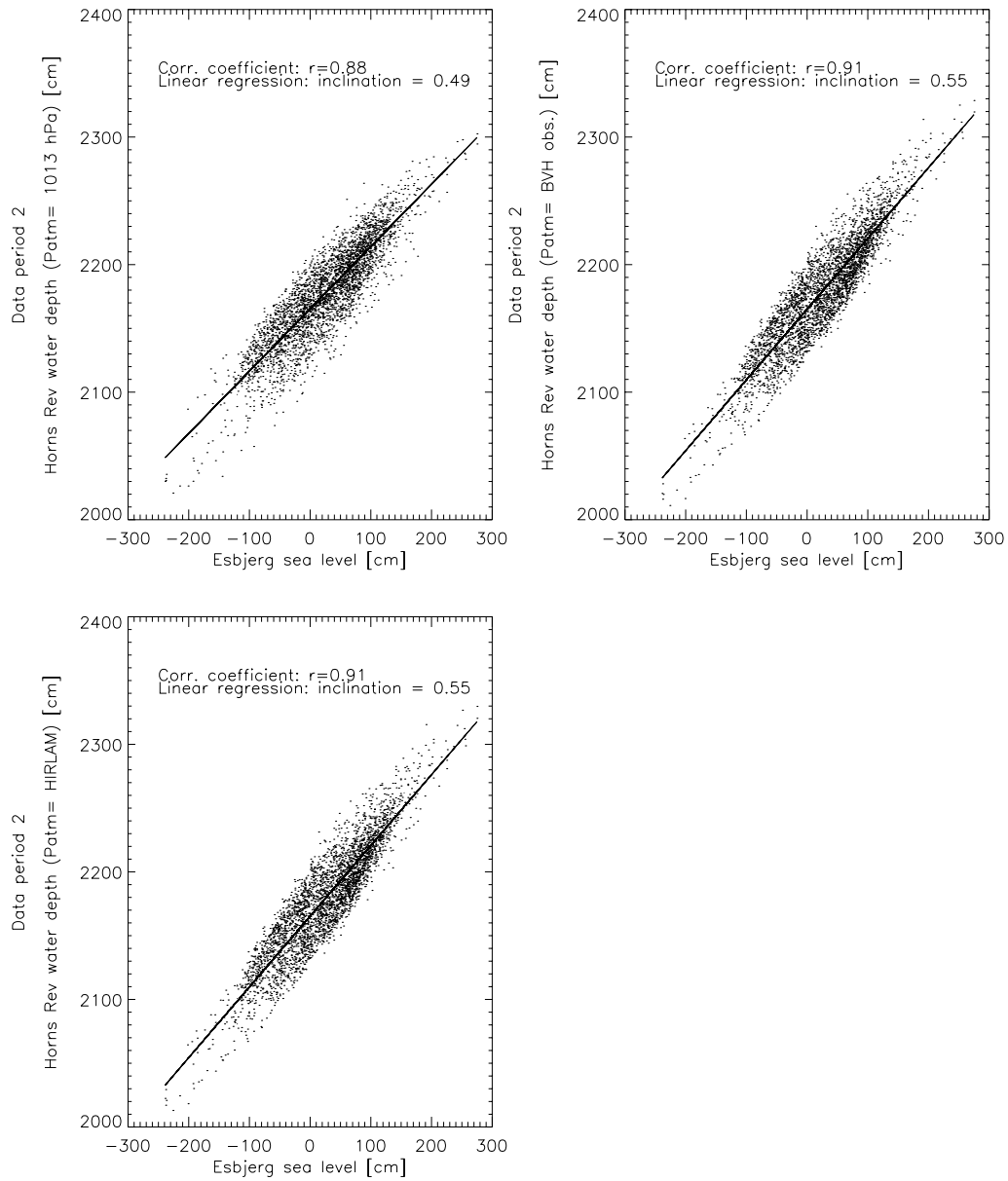


Figure A.3: As Fig. A.2 but for data period 2.

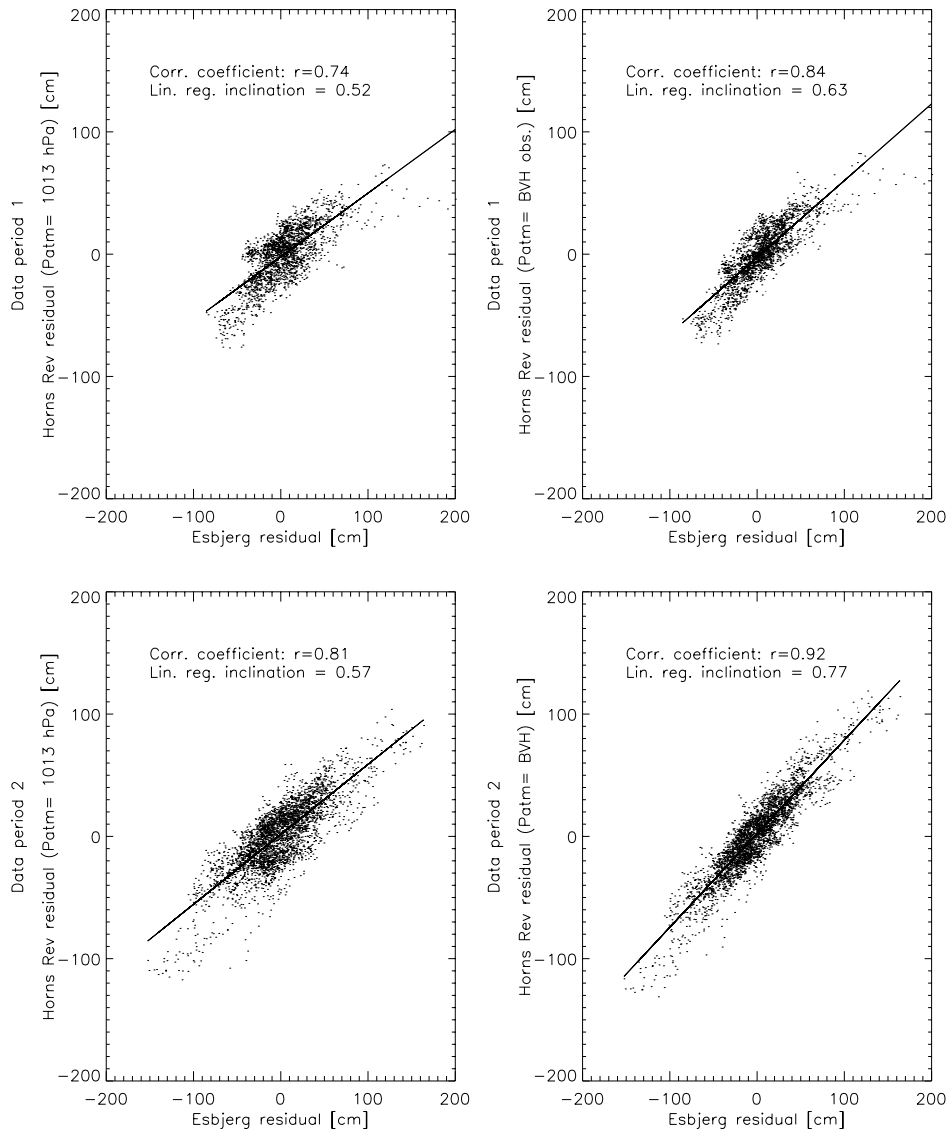


Figure A.4: Scatter plot of Horns Rev residuals calculated with atmospheric pressure observations from the synop station at Blåvands Huk (BVH) as function of residuals from the coastal tide gauge station at Esbjerg.

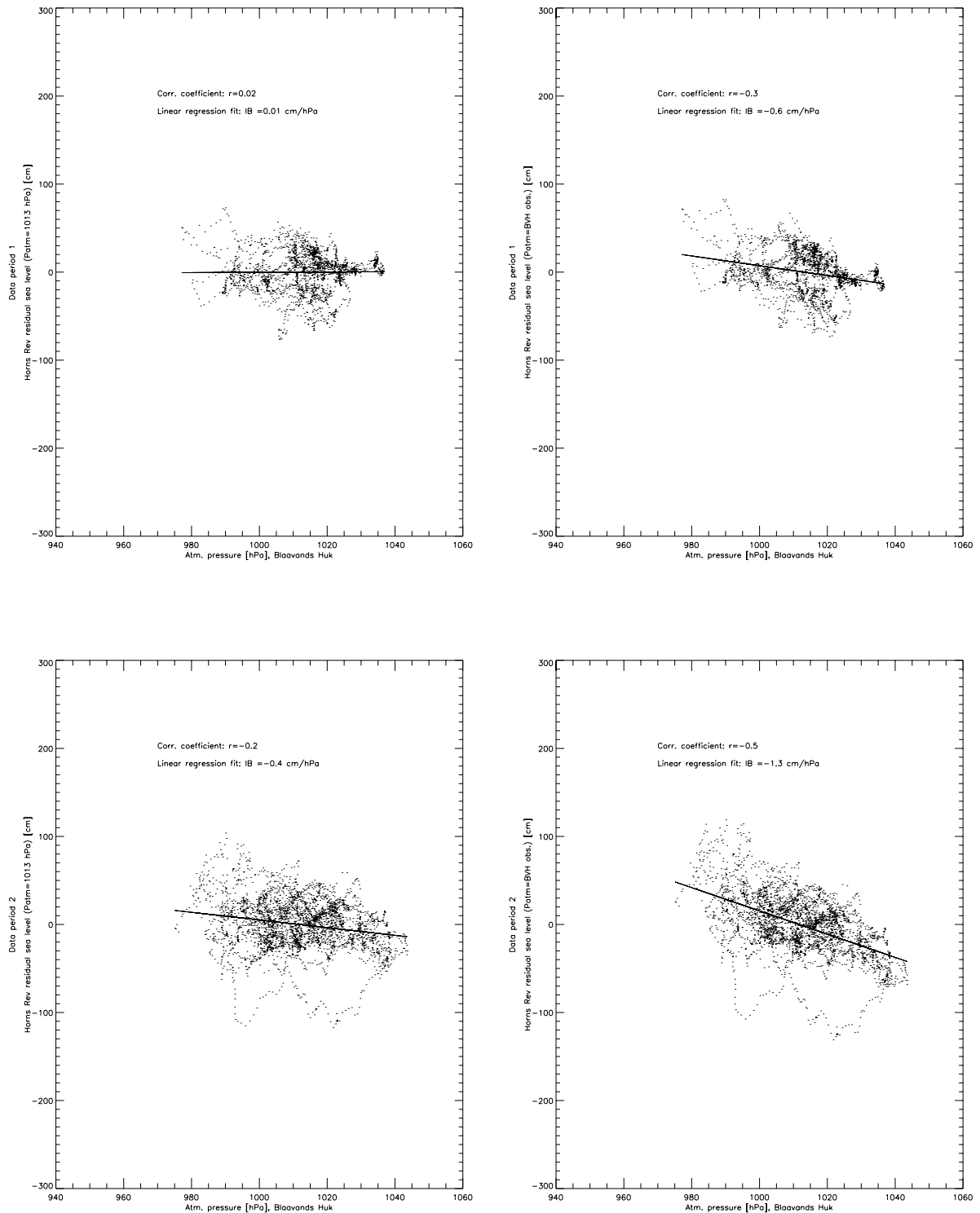


Figure A.5: Scatter plot of Horns Rev residuals plotted as function of the atmospheric pressure observations from Blåvands Huk. The sea level residuals are plotted for data period 1 at top, and data period 2 at bottom.

Appendix B

The M_2 Modulation Wave

A linear combination of the harmonics for the M_2 constituent and its two neighbouring constituents MA_2 and MB_2 gives (the nodal corrections are ignored):

$$\begin{aligned} h(t) &= A_{M_2} e^{i(\omega_{M_2}t - g_{M_2} + V_{M_2})} + A_{MA_2} e^{i(\omega_{MA_2}t - g_{MA_2} + V_{MA_2})} + A_{MB_2} e^{i(\omega_{MB_2}t - g_{MB_2} + V_{MB_2})} \\ &= e^{i(\omega_{M_2}t - g_{M_2} + V_{M_2})} \times \left[A_{M_2} + A_{MA_2} e^{i(-\Delta\omega t + g_{M_2} - g_{MA_2} + V_{MA_2} - V_{M_2})} \right. \\ &\quad \left. + A_{MB_2} e^{i(\Delta\omega_{MB_2}t - \omega_{M_2}t + g_{M_2} - g_{MB_2} + V_{MB_2} - V_{M_2})} \right] \end{aligned}$$

where A , ω , g and V are the amplitude, frequency, phase lag and the astronomical argument, respectively, for each of the three constituents, and $\Delta\omega = \omega_{M_2} - \omega_{MA_2} = \omega_{MB_2} - \omega_{M_2}$. Taking the real part of the expression gives

$$\begin{aligned} h(t) &= \cos(\omega_{M_2}t - g_{M_2} + V_{M_2}) \times \\ &\quad \left[A_{M_2} + A_{MA_2} \cos(-\Delta\omega t + g_{M_2} - g_{MA_2} + V_{MA_2} - V_{M_2}) \right. \\ &\quad \left. + A_{MB_2} \cos(\Delta\omega t + g_{M_2} - g_{MB_2} + V_{MB_2} - V_{M_2}) \right] \\ &- \sin(\omega_{M_2}t - g_{M_2} + V_{M_2}) \times \\ &\quad \left[A_{MA_2} \sin(-\Delta\omega t + g_{M_2} - g_{MA_2} + V_{MA_2} - V_{M_2}) \right. \\ &\quad \left. + A_{MB_2} \sin(\Delta\omega t + g_{M_2} - g_{MB_2} + V_{MB_2} - V_{M_2}) \right] \\ &= \left[A_{M_2} + S(t) \right] \times \cos(\omega_{M_2}t - g_{M_2} + V_{M_2}) - R(t) \times \sin(\omega_{M_2}t - g_{M_2} + V_{M_2}) \end{aligned}$$

where $S(t)$ is given by

$$\begin{aligned} S(t) &= A_{MA_2} \cos(-\Delta\omega t - (g_{MA_2} - g_{M_2}) + V_{MA_2} - V_{M_2}) \\ &\quad + A_{MB_2} \cos(\Delta\omega t - (g_{MB_2} - g_{M_2}) + V_{MB_2} - V_{M_2}), \end{aligned}$$

and $R(t)$ by

$$R(t) = A_{MA_2} \sin(-\Delta\omega t - (g_{MA_2} - g_{M_2}) + V_{MA_2} - V_{M_2}) \\ + A_{MB_2} \sin(\Delta\omega t - (g_{MB_2} - g_{M_2}) + V_{MB_2} - V_{M_2}) .$$

The linear combination of the M_2 , MA_2 and MB_2 harmonics is seen to result in a M_2 carrier wave with a modulation in the amplitude at a period of $T \approx 1$ year, plus a small term at the M_2 frequency but with the phase lag shifted 90° . The modulation wave $S(t)$ has been used in Chapter 4 to investigate the annual modulation of the M_2 constituent. The sine term is considered as a small perturbation term to the annual modulation of the M_2 wave due to the 90° phase shift, and has not been included in the investigations.

Appendix C

Vector Root-Sum-Square

The total error of the difference between two vectors is given by the length of the vector difference integrated over one period:

$$\begin{aligned} RSS_{vector} &= \left[\frac{1}{N} \sum_{i=1}^N \frac{1}{T} \int_0^T \| A_{TG} e^{i(\omega t - g_{TG})} - A_{2D} e^{i(\omega t - g_{2D})} \|^2 dt \right]^{1/2} \\ &= \left[\frac{1}{N} \sum_{i=1}^N \frac{1}{T} \int_0^T \left(\left(A_{TG} \cos(\omega t - g_{TG}) - A_{2D} \cos(\omega t - g_{2D}) \right)^2 \right. \right. \\ &\quad \left. \left. + \left(A_{TG} \sin(\omega t - g_{TG}) - A_{2D} \sin(\omega t - g_{2D}) \right)^2 \right) dt \right]^{1/2} \\ &= \left[\frac{1}{N} \sum_{i=1}^N \frac{1}{T} \int_0^T \left(A_{TG}^2 + A_{2D}^2 - 2A_{TG}A_{2D} \cos(\omega t - g_{TG}) \cos(\omega t - g_{2D}) \right. \right. \\ &\quad \left. \left. - 2A_{TG}A_{2D} \sin(\omega t - g_{TG}) \sin(\omega t - g_{2D}) \right) dt \right]^{1/2} \\ &= \left[\frac{1}{N} \sum_{i=1}^N \frac{1}{T} \int_0^T \left(A_{TG}^2 + A_{2D}^2 - A_{TG}A_{2D} \left[\cos(-g_{TG} + g_{2D}) + \cos(2\omega t - g_{TG} - g_{2D}) \right] \right. \right. \\ &\quad \left. \left. - A_{TG}A_{2D} \left[\cos(-g_{TG} + g_{2D}) - \cos(2\omega t - g_{TG} - g_{2D}) \right] \right) dt \right]^{1/2} \\ &= \left[\frac{1}{N} \sum_{i=1}^N \frac{1}{T} \int_0^T \left(A_{TG}^2 + A_{2D}^2 - 2A_{TG}A_{2D} \cos(g_{TG} - g_{2D}) \right) dt \right]^{1/2} \\ &= \left[\frac{1}{N} \sum_{i=1}^N \left(A_{TG}^2 + A_{2D}^2 - 2A_{TG}A_{2D} \cos(g_{TG} - g_{2D}) \right) \right]^{1/2} \\ &= \left[\frac{1}{N} \sum_{i=1}^N \frac{1}{2} \left[\left(A_{TG} \cos(g_{TG}) - A_{2D} \cos(g_{2D}) \right)^2 + \left(A_{TG} \sin(g_{TG}) - A_{2D} \sin(g_{2D}) \right)^2 \right] \right]^{1/2} \end{aligned}$$

where the sum i is made over the total set of data, N .

Appendix D

The Modulation Wave from the NEAC 2D-model T runs

The modulation wave calculated from the NEAC 2D-model T runs are shown below for the years 1992-1997, for the model grid points corresponding to the location of the tide gauge stations around the North Sea. The amplitude of the modulation wave are shown in absolute values [cm] and relative to the M_2 amplitude. Also shown is the phase lag for the M_2 maximum with 0° corresponding to January 1 and 360° to December 31. These tables are to be compared with Table 4.7 for the T+S runs.

1992	M_2 [cm]	S(t) [cm]	S(t) [%]	S(t) [°]
Wick	117.2	0.2	0.2	180.5
Leith	190.2	0.4	0.2	177.6
North Shields	163.6	0.4	0.2	176.8
Lowestoft	69.3	0.2	0.3	173.8
Sheerness	189.1	0.5	0.3	167.7
Esbjerg	65.1	0.3	0.5	164.8
Hvide Sande	26.8	0.2	0.7	169.5
Hanstholm	11.2	0.2	1.8	169.1
Hirtshals	13.2	0.3	2.3	169.0

1993	M_2 [cm]	S(t) [cm]	S(t) [%]	S(t) [°]
Wick	117.0	0.5	0.4	172.8
Leith	189.7	0.9	0.5	174.2
North Shields	163.1	0.8	0.5	174.3
Lowestoft	69.1	0.4	0.6	179.2
Sheerness	187.7	1.5	0.8	174.7
Esbjerg	64.6	0.5	0.8	175.7
Hvide Sande	26.7	0.2	0.7	181.3
Hanstholm	11.2	0.1	0.9	195.8
Hirtshals	13.2	0.1	0.8	196.6

1994	M_2 [cm]	S(t) [cm]	S(t) [%]	S(t) [°]
Wick	116.9	0.5	0.4	182.7
Leith	189.5	0.9	0.5	184.6
North Shields	162.9	0.7	0.4	185.3
Lowestoft	69.1	0.3	0.4	189.2
Sheerness	187.0	1.4	0.7	192.1
Esbjerg	64.2	0.5	0.8	196.5
Hvide Sande	26.5	0.1	0.4	202.7
Hanstholm	11.1	0.1	0.9	238.8
Hirtshals	13.0	0.1	0.8	238.7

1995	M_2 [cm]	S(t) [cm]	S(t) [%]	S(t) [°]
Wick	117.3	0.8	0.7	351.3
Leith	190.3	1.3	0.7	350.3
North Shields	163.5	1.1	0.7	349.5
Lowestoft	69.4	0.5	0.7	351.2
Sheerness	187.3	0.8	0.4	328.8
Esbjerg	64.2	0.3	0.5	323.6
Hvide Sande	26.5	0.2	0.8	342.8
Hanstholm	11.0	0.1	0.9	338.4
Hirtshals	12.9	0.0	0.0	327.4

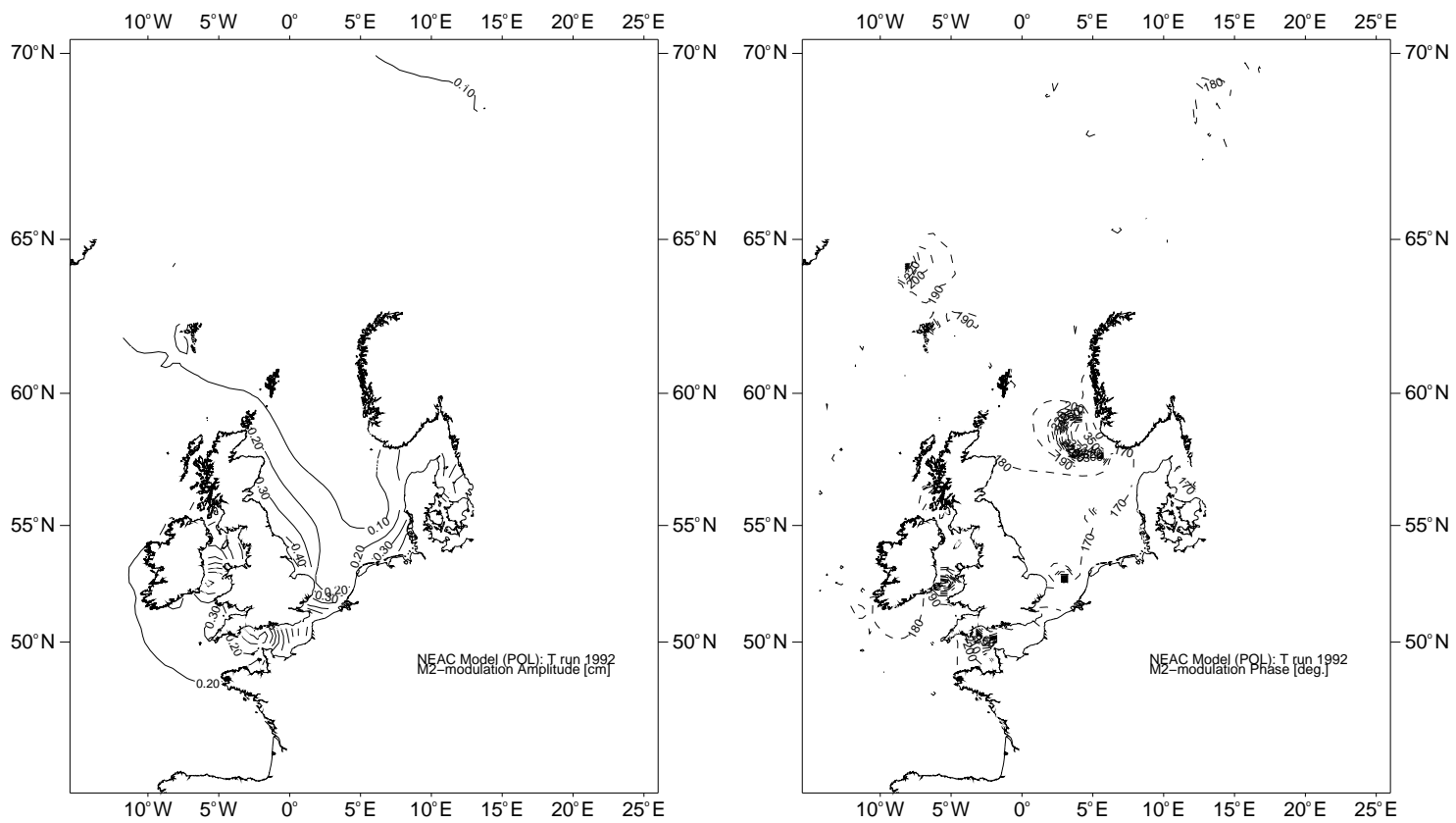
1996	M_2 [cm]	S(t) [cm]	S(t) [%]	S(t) [°]
Wick	116.7	0.3	0.3	180.8
Leith	189.3	0.5	0.3	179.5
North Shields	162.6	0.5	0.3	179.5
Lowestoft	68.9	0.3	0.4	173.7
Sheerness	186.2	0.4	0.2	178.7
Esbjerg	63.7	0.2	0.3	170.9
Hvide Sande	26.3	0.2	0.8	169.6
Hanstholm	10.8	0.2	1.9	166.1
Hirtshals	12.6	0.2	1.6	165.9

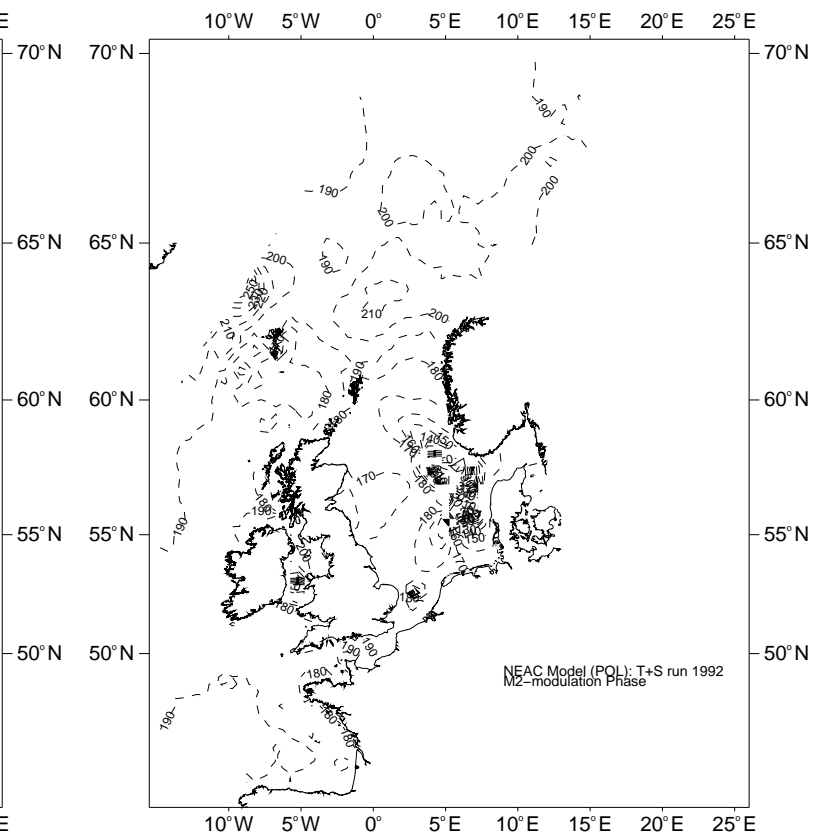
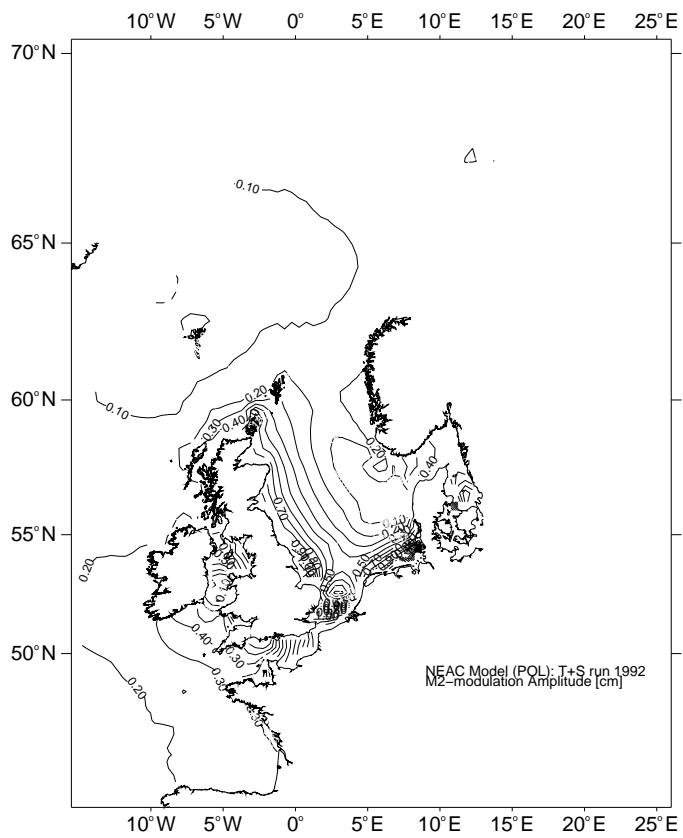
1997	M_2 [cm]	S(t) [cm]	S(t) [%]	S(t) [°]
Wick	116.6	0.5	0.4	170.1
Leith	189.0	0.9	0.5	171.0
North Shields	162.4	0.8	0.5	170.8
Lowestoft	68.8	0.4	0.6	174.4
Sheerness	185.5	1.4	0.8	169.4
Esbjerg	63.5	0.4	0.6	166.3
Hvide Sande	26.3	0.1	0.4	167.1
Hanstholm	10.8	0.1	0.9	170.5
Hirtshals	12.7	0.1	0.8	172.7

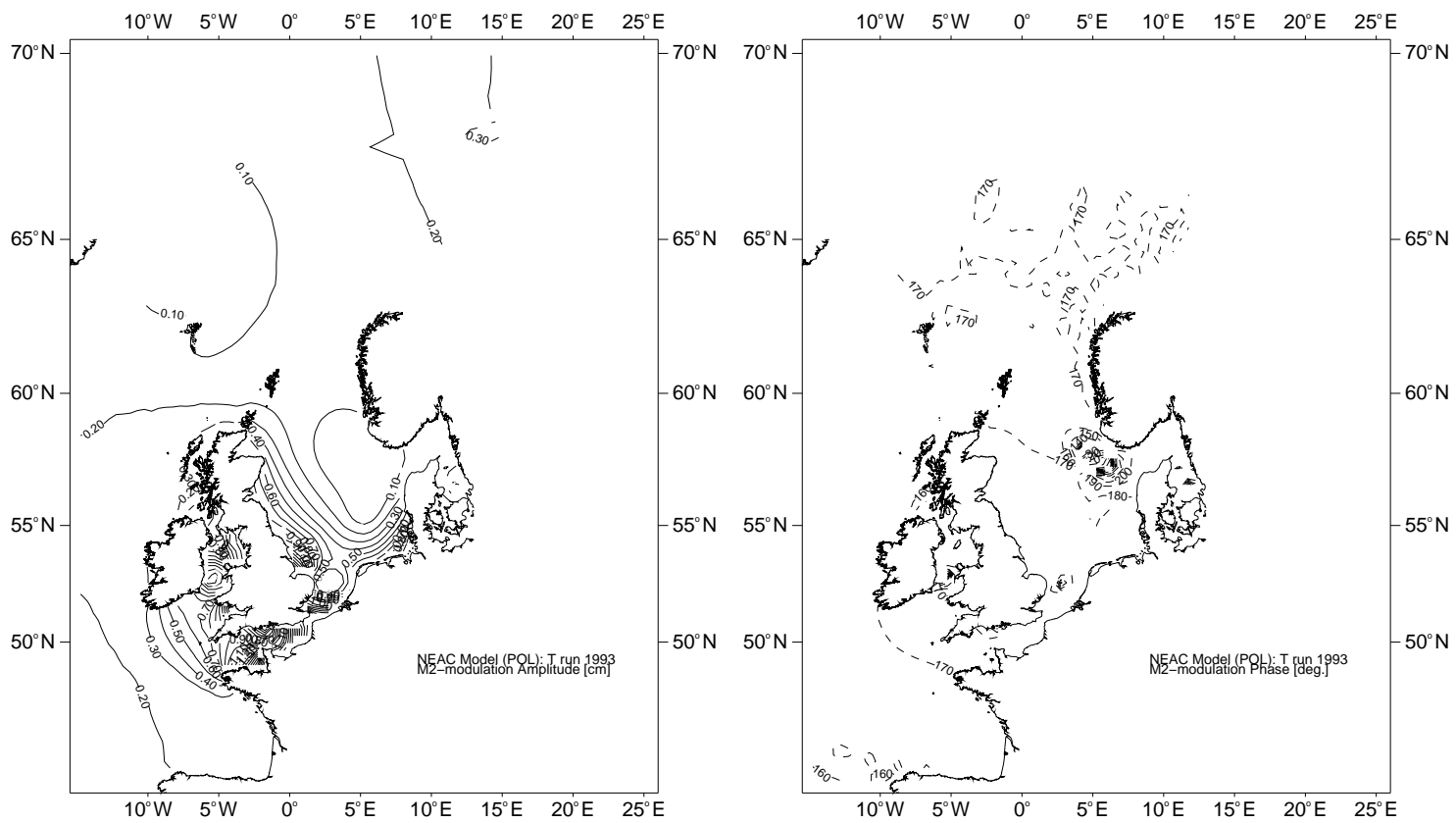
Appendix E

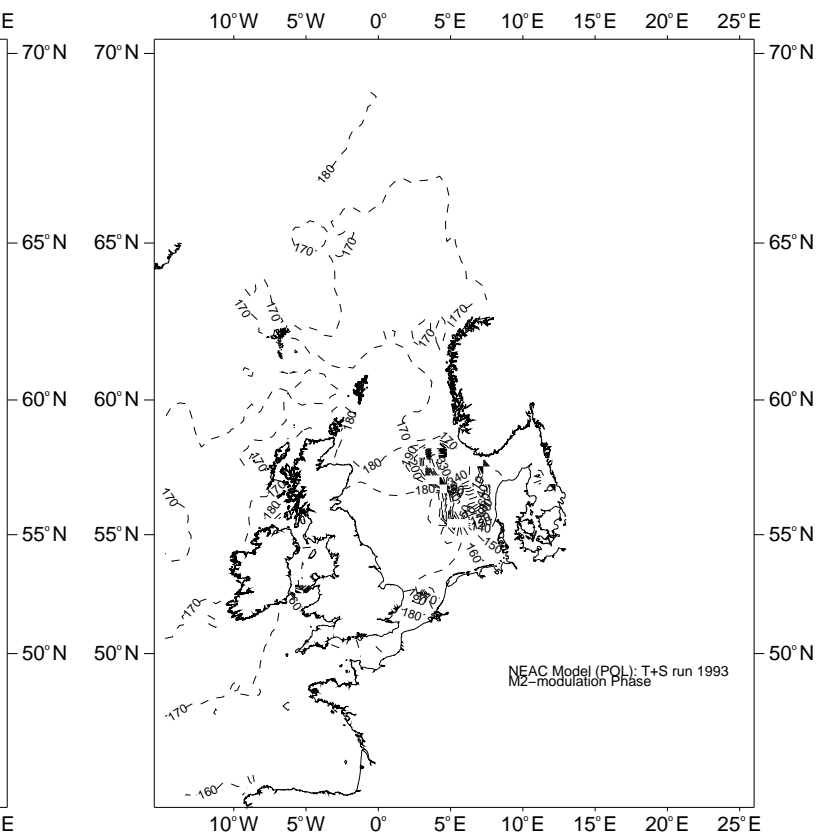
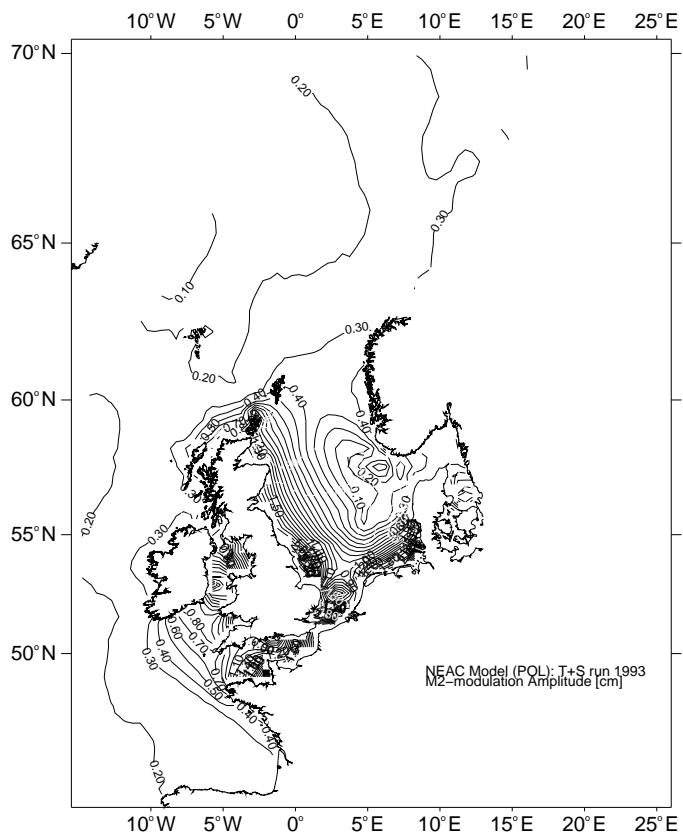
Plots of the NEAC 2D-model Modulation Wave

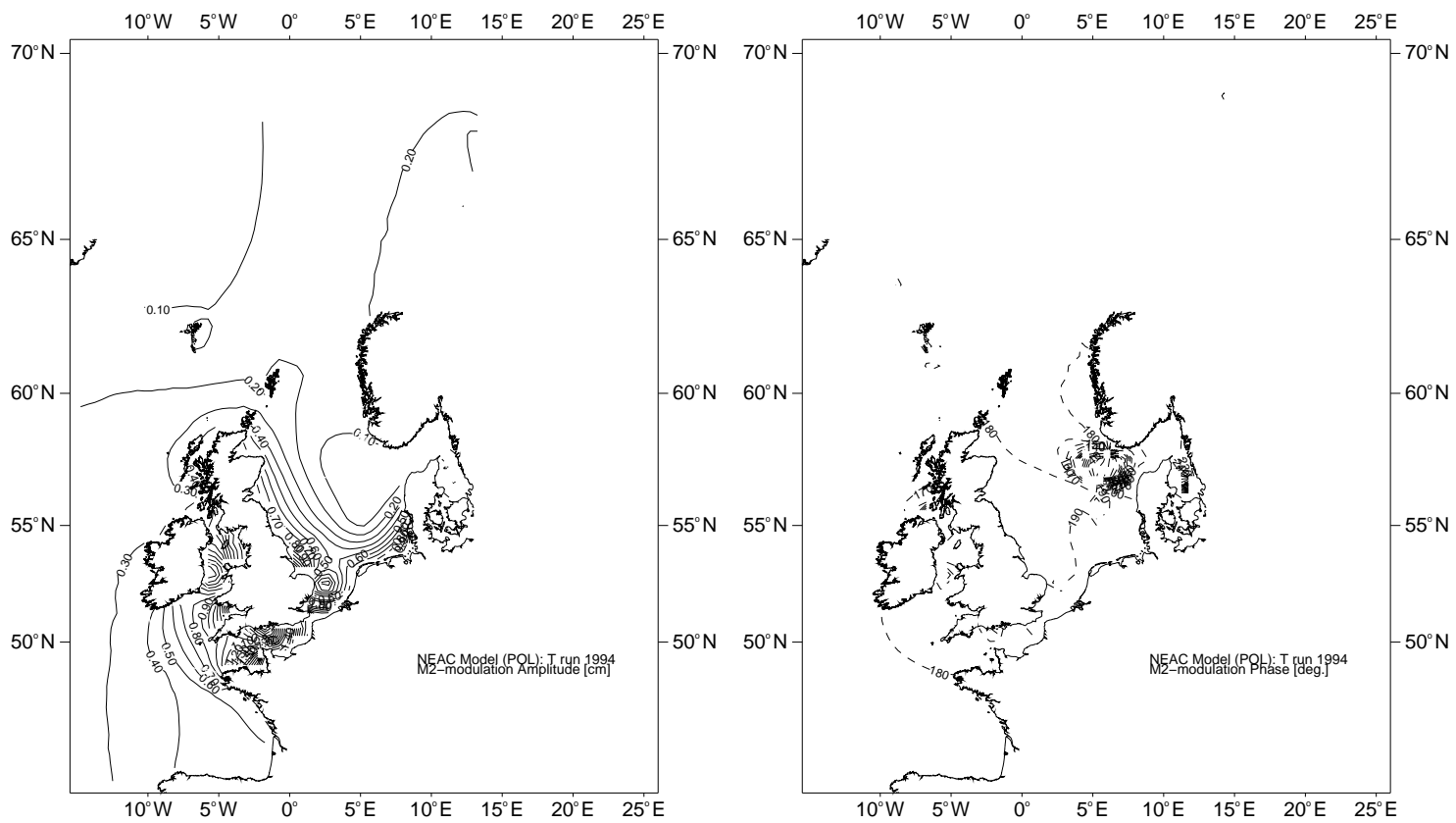
On the following pages are shown the modulation wave, $S(t)$ calculated from the 2D barotropic numerical model (described in Section 4.5.1). The amplitude for the modulation wave is given in cm and the time in the year for this maximum is given in degrees and plotted for the years 1992-1997 for runs forced with tides only (T runs) and forced with both tides and atmospheric forcing fields (T+S runs).

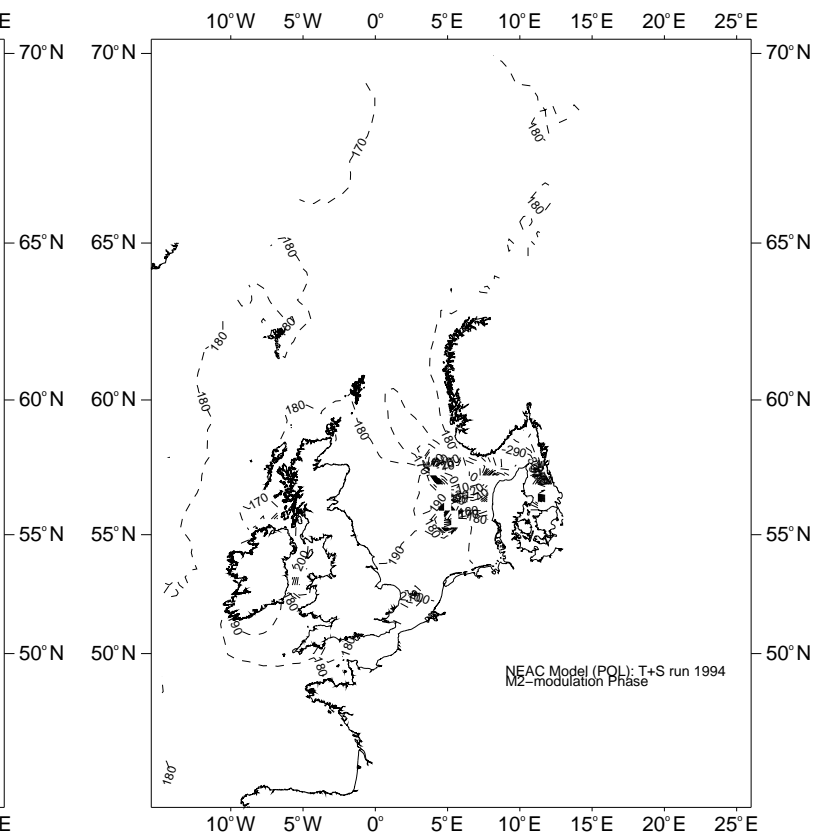
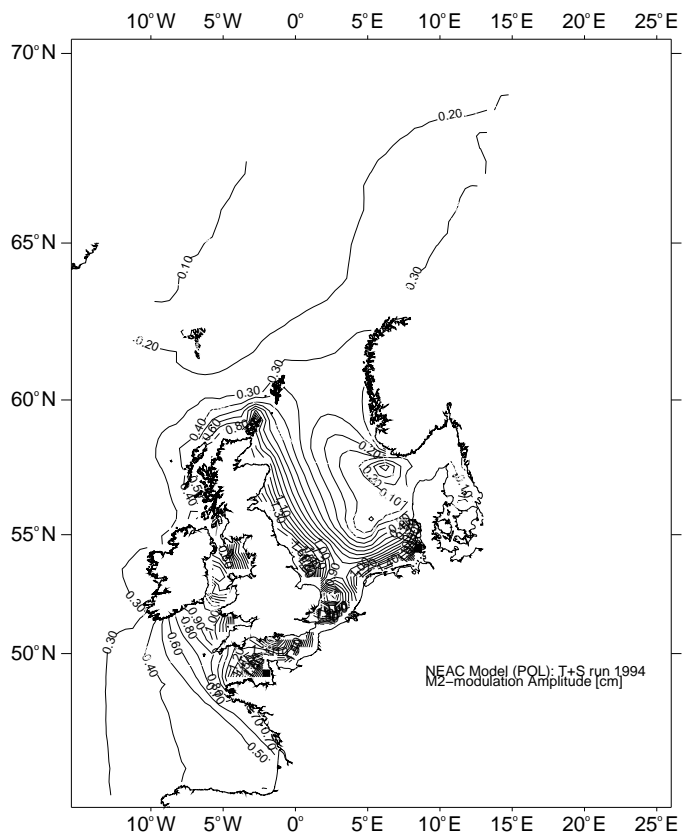


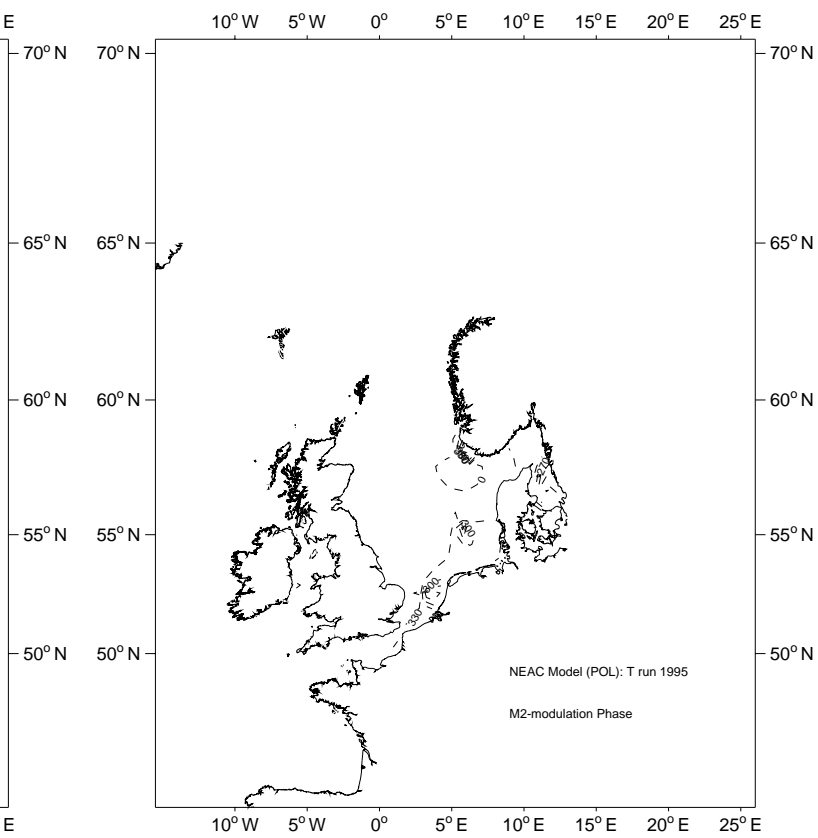
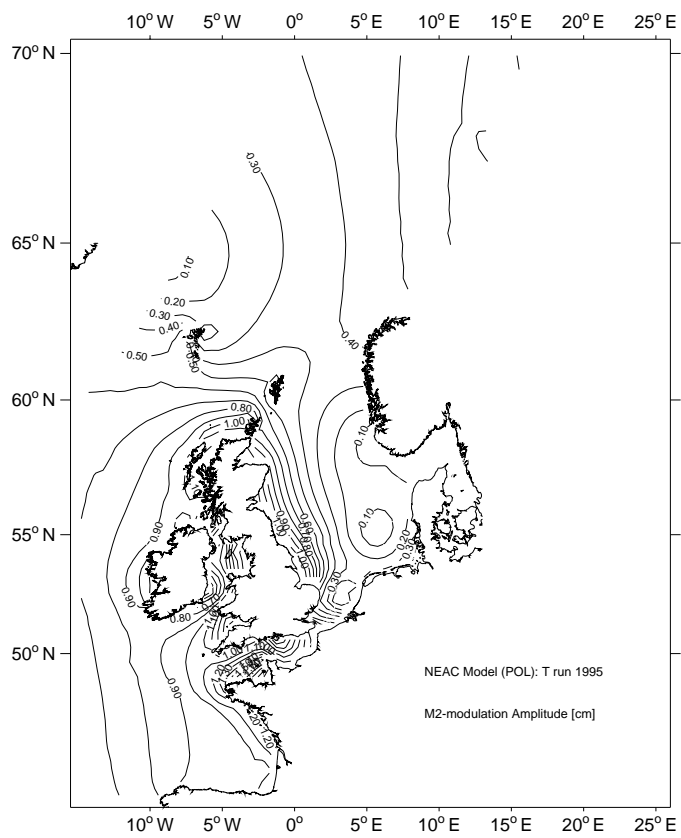


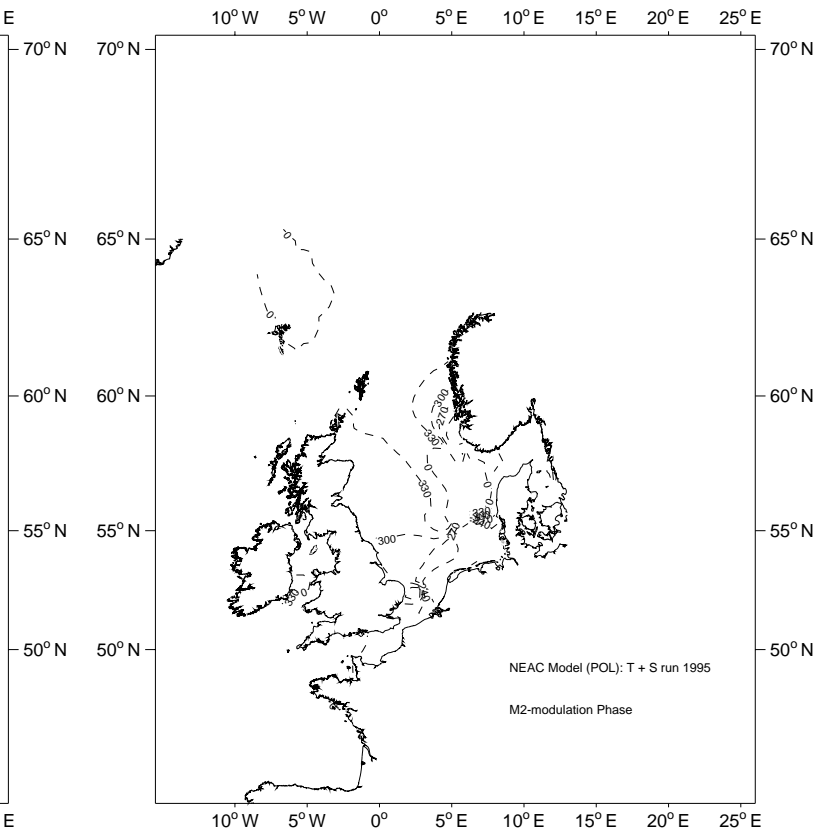
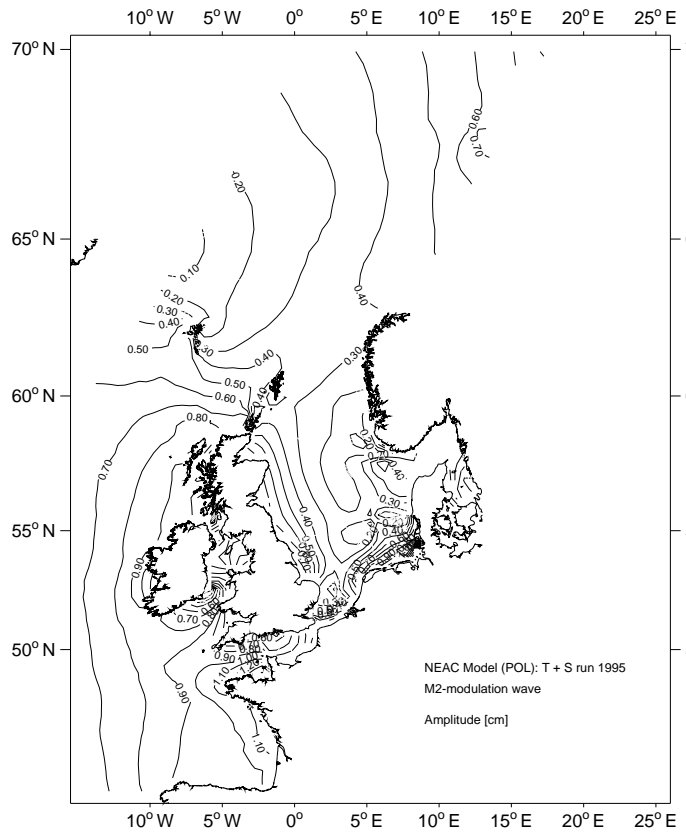


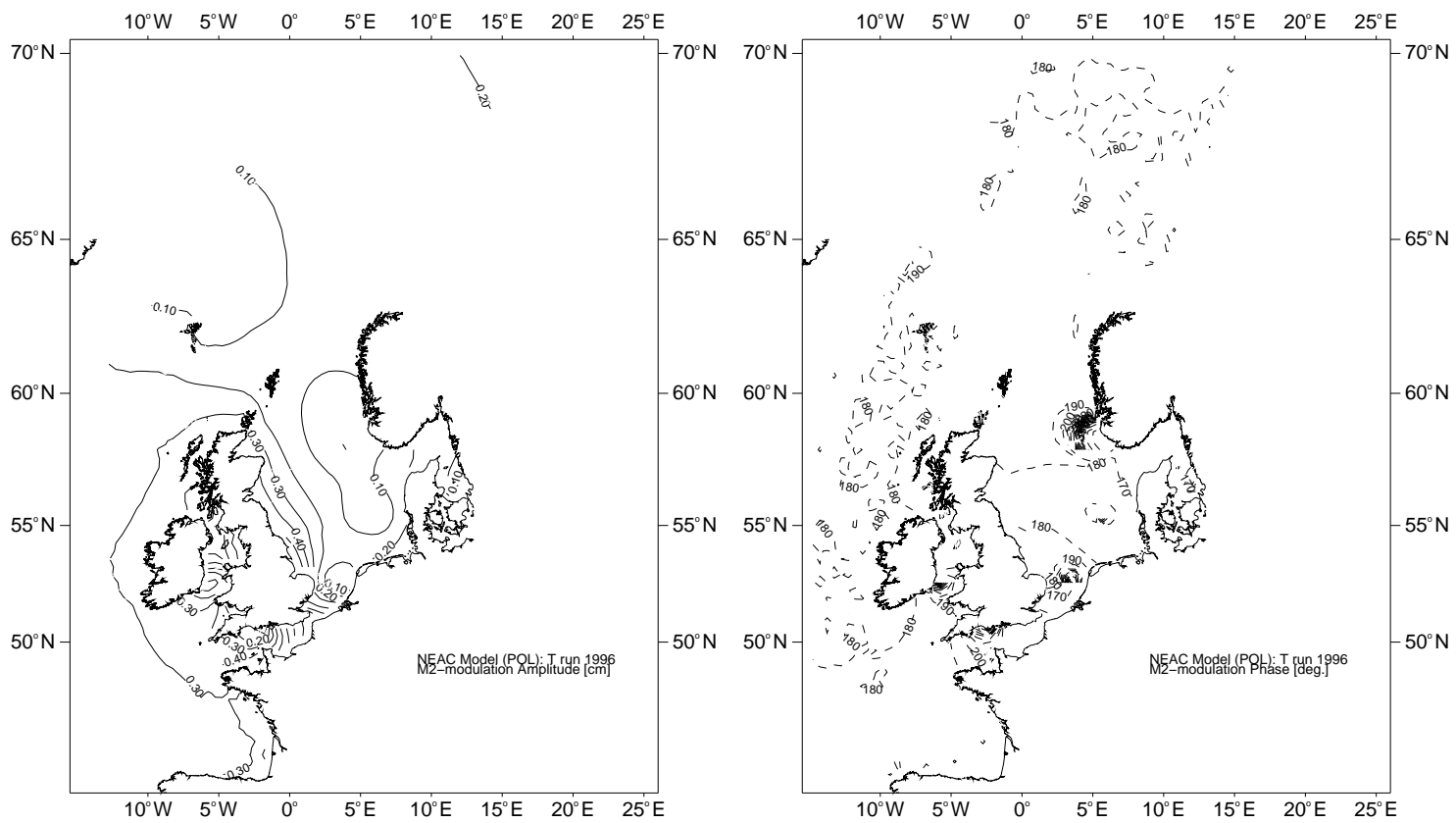


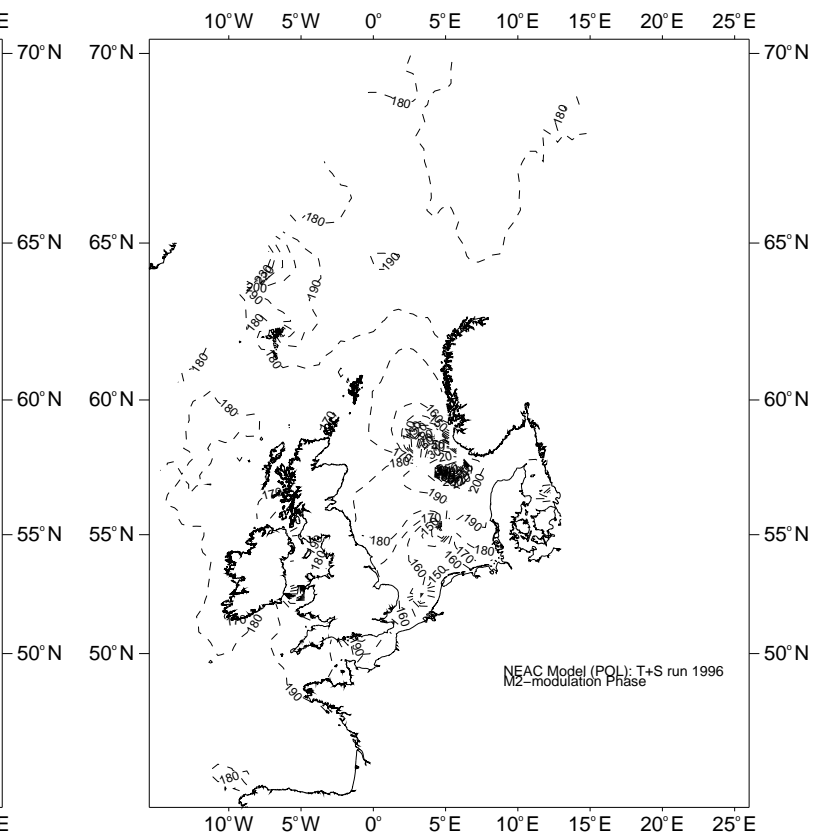
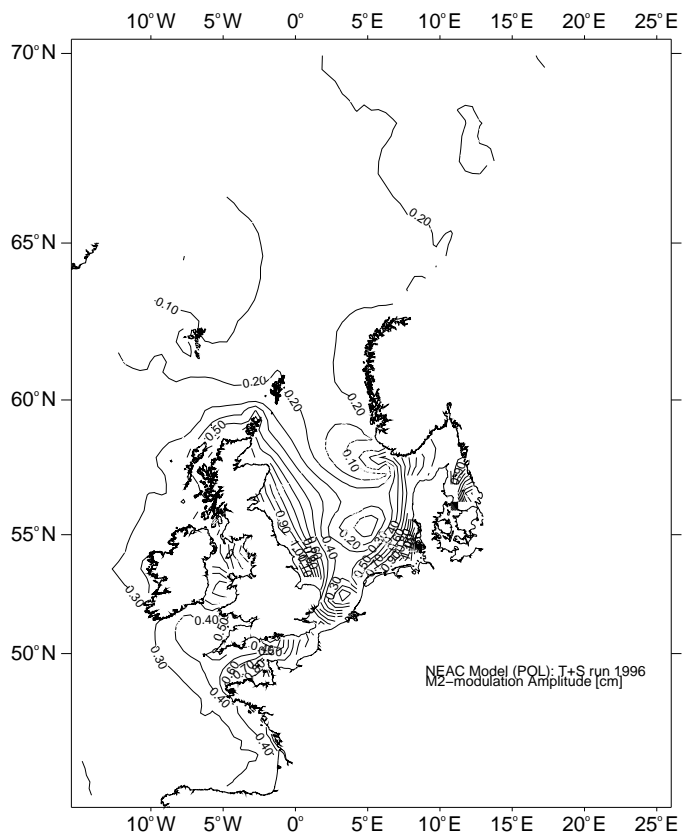


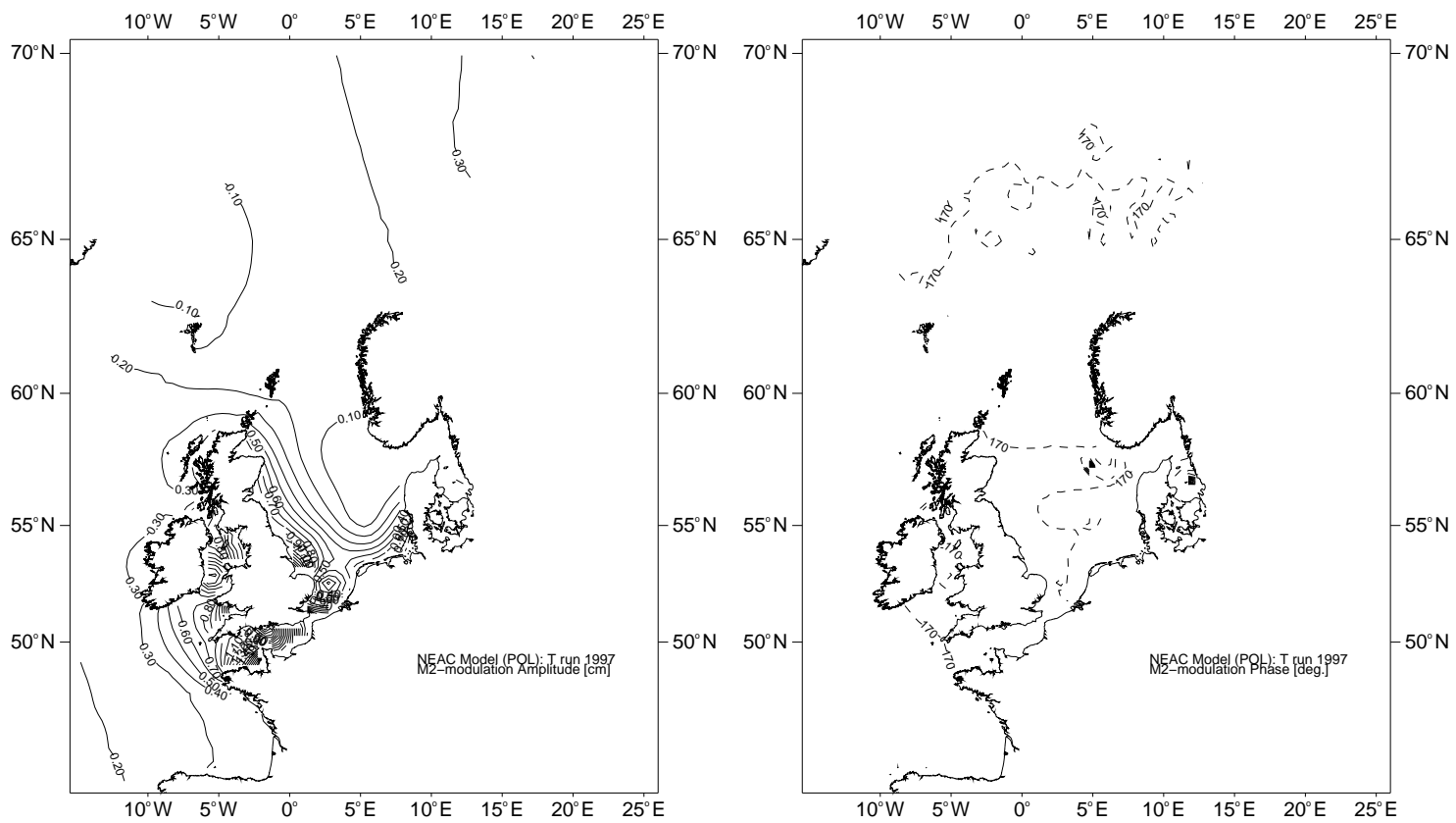


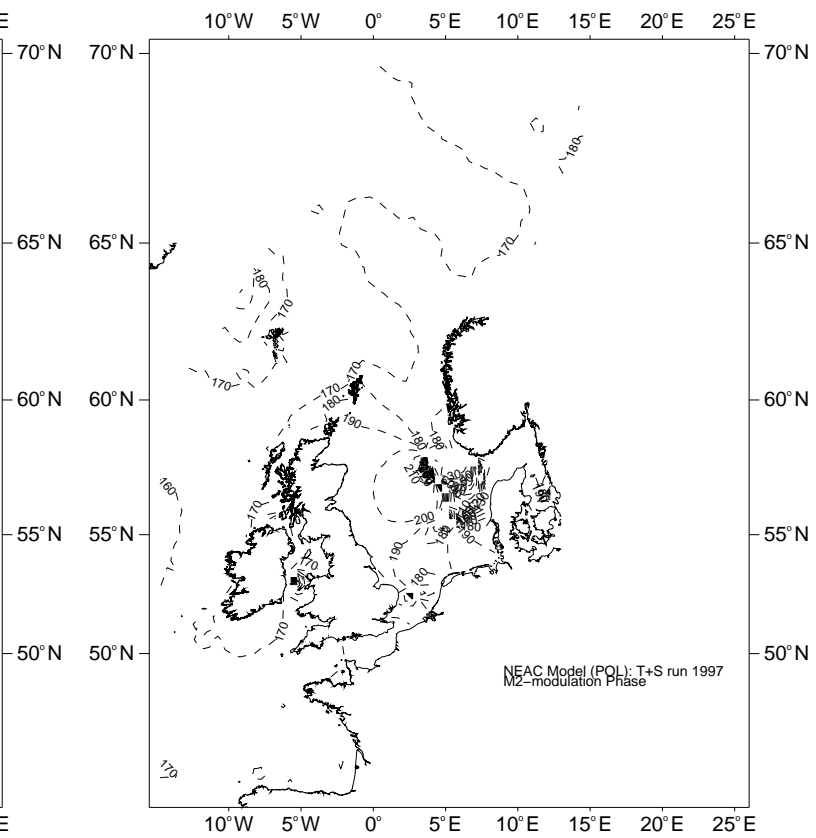
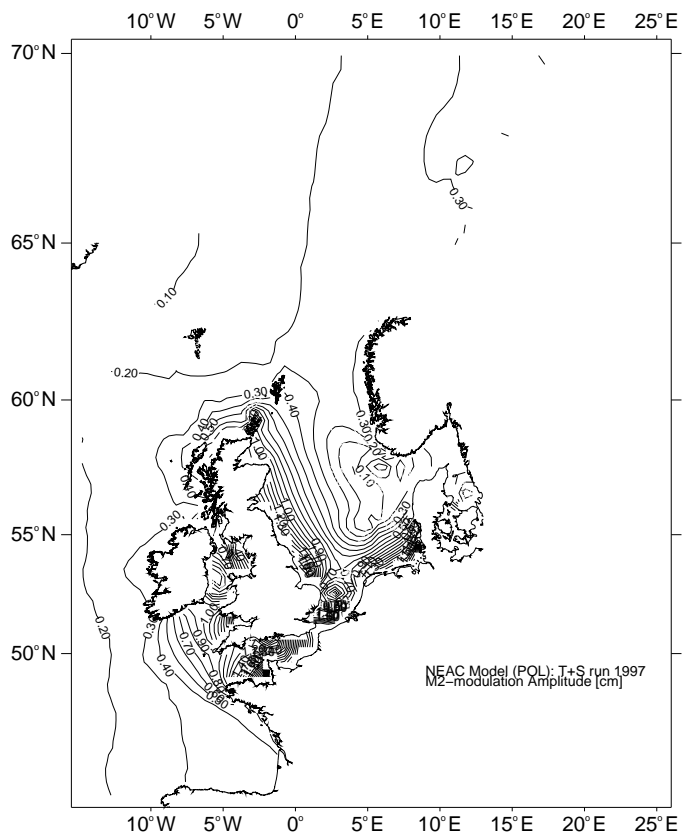












Appendix F

Paper submitted to Geophysical Research Letters

The enclosed paper has been accepted by Geophysical Research Letters, November 2000, and is published in Geophysical Research Letters, Vol. 28, NO. 4, pages 567-570, February 2001.

Seasonal Variation in the Main Tidal Constituent from Altimetry

V. Huess

Danish Meteorological Institute, Copenhagen, Denmark

O. B. Andersen

National Survey and Cadastre, Copenhagen, Denmark

Abstract

The existence of seasonal variations in the main tidal constituents has been known for a long time from coastal tide gauges. In this paper we extend the amount of observations from the relatively limited number of coastal tide gauge observations to also include the large amount of offshore information that have become available from altimetry. These observations are compared with results from a hydrodynamical model applied for the north-west European shelf. The model clearly identifies the seasonal variation in the M_2 constituent as a shallow water effect with a large part of the variation explained as a barotropic signal having high dependency on the meteorological field over the area.

Introduction

Seasonal variation in the main tidal constituents have been known for a long time. In 1934 R. H. Corkan investigated tide gauge data from the station in Liverpool, U.K., and observed less tidal range in the winter period than predicted, and higher tidal range in the summer period than predicted [Corkan, 1934]. To account for this observed annual perturbation, Corkan included two small semi-diurnal constituents, MA_2 and MB_2 , that loses and gains approximately 1° in the phase lag per day on M_2 , respectively. Cartwright, [1968] identified two causes to the existence of the MA_2 and MB_2 constituents, and defined an *annual* modulation in M_2 caused by a pure gravitational effect (the anomalistic year with the period $T=365.2596$ days), and a *seasonal* modulation caused by the solar inclination (the tropical year with the period $T=365.2422$ days). The annual contribution to the constituents MA_2 and MB_2 are calculated from the gravity potential corresponding to 0.345% and 0.305% of the M_2 amplitude, respectively [Cartwright and Taylor, 1971]. The distribution and cause of the observed MA_2 and MB_2 amplitudes on several percent of the M_2 wave, have previously been investigated from coastal tide gauge data mainly located around the British Isles [Baker and Alcock, 1983; Pugh and Vassie, 1976; Pugh and Vassie, 1994]. New information about shallow water tides have recently been obtained from altimetry data in the north-west European shelf region [Andersen, 1999]. We extend the previous investigations of the seasonal modulation of the M_2 constituent to include the large amount of offshore sea level observations from altimetry (see Figure 1). This combined offshore and onshore data set is compared with results from a hydrodynamical model, with the objective to investigate the main factors responsible for the seasonal variation in M_2 .

Figure 1

Seasonal Variation in the M_2 Constituent

A linear combination of the three harmonics M_2 , MA_2 and MB_2 can be shown to give a main contribution that can be interpreted as a M_2 carrier wave plus a modulation wave with a modulation in the M_2 amplitude at a period of $T = \frac{1}{\Delta\omega} \approx 1$ year (Woodworth et al. [1991])

$$h(t) \approx [H_{M_2} + S(t)] e^{i(\omega_{M_2}t - g_{M_2} + V_{M_2})},$$

where the modulation wave $S(t)$ is given by

$$S(t) = H_{MA_2} e^{i(-\Delta\omega t - g_{MA_2} + g_{M_2} - 280.19^\circ)} + H_{MB_2} e^{i(\Delta\omega t - g_{MB_2} + g_{M_2} + 280.19^\circ)},$$

where H is the amplitude, ω the frequency, g the phase lag, and V the astronomical argument for the three constituents. Nodal corrections are ignored. The seasonal variation in the M_2 constituent is calculated by the modulation wave $S(t)$. Note, that a separation of the *annual* and the *seasonal* contributions according to Cartwrights definitions is not possible due to the very small separation in the frequency band, and the name seasonal variation will be used throughout this paper to designate the total variation, where this term then includes the annual contribution.

Altimeter Data

Five years of TOPEX/POSEIDON altimetry (184 cycles) were used to provide offshore observations of the sea level height variations. Data were provided by the NASA Pathfinder Data. The altimetric observations were processed using the set of provided standard geophysical, media and instrumental corrections. A special version without tidal correction were provided. Subsequently data within 2° by 3° latitude by longitude bins were analysed for the tidal signal using a harmonic analysis for the largest four constituents. Information about the time of observation within the year were taken into account by selecting data in a 3 month data window, shifted by 10 days through the year computing ocean tide parameters for each 10 days shift. The choice of a 3 month data window was chosen to ensure an adequate number of observations within each time shift. Plate 1 shows the maximum deviation from the mean M_2 amplitude (top), and the corresponding phase in the year for this maximum (bottom), with 0° at January 1st. The T/P data identify an annual signal in the M_2 amplitude in the south eastern part of the North Sea ranging up to 5.0 cm in July. This corresponds to deviations of up to 8% of the M_2 amplitude, and indicates a strong seasonal variation in this region. Harmonic analysis of five years of tide gauge data from Esbjerg and Cuxhaven is shown in Figure 2 (for location see Figure 1). Calculations of the seasonal variation $S(t)$ for Esbjerg and Cuxhaven for the investigated years gives maximum deviations in May of 2.3 cm and 7.8 cm corresponding to 3% and 6% of the M_2 amplitude, respectively. This corresponds relatively well with the altimetric results in Plate 1.

Plate 1

Figure 2

Model Data

Five years of model simulations (1992-1996) from the 35 km barotropic and non linear shallow water hydrodynamical model developed by R. A. Flather, Proudman Oceanographic Laboratory (POL), U.K. [Flather, 1976] were used to investigate the causing factors of the seasonal variation in M_2 . To investigate the effect from the interaction with the meteorological field, data from model runs forced with tides only and model runs forced with both tides and meteorological fields were analyzed. The tidal forcing consists of a tidal wave generated by 26 tidal constituents (MA_2 and MB_2 are not included in the forcing) at the open boundaries. The meteorological forcing consists of reanalyzed fields from the Norwegian Meteorological Institute [Reistad and Iden, 1998]. The seasonal modulation wave $S(t)$ simulated by the model for one year (1992) is shown in Plate 2. Maximum amplitude and corresponding phase lag for $S(t)$ are shown. The maximum deviation for 1992 is a little more than 2 cm. For 1994 a maximum of more than 3 cm is found in German Bight. The seasonal variation is in the tidal run caused by a non linear combination between the tidal frequencies, but the model does not resolve which constituents interact to give the effect. By comparing the two model runs, the seasonal variation can be identified as a shallow water effect with a significant dependence on the meteorological forcing.

Plate 2

Model Results and Validation

The strong signal in the south eastern part of the North Sea, having a maximum M_2 deviation in the boreal summer period is observed from both altimetry and the hydrodynamical model. The different spatial shape of the model and the T/P derived signal may be explained by the poor spatial resolution of the T/P data (processed in 2° by 3° bins). This is also the explanation for the missing seasonal modulation in the T/P observations along the British east coast. Results from the five years model simulations have been validated by 12 tide gauges along the North Sea coast (Wick, Leith, North Shields, Lowestoft, Sheerness, Roscoff, Cherbourg, Oostende, Esbjerg, Torsminde, Hanstholm and Hirtshals). The model forced with both tides and meteorological fields captures on average 60% of the M_2 seasonal variation at these tide gauges. Without the meteorological forcing, 40% of the variation was explained by the non linear tidal interaction in the model. This identifies a strong dependence to both the tidal interaction and the tidal-

meteorological interaction. Furthermore the model captures the large inter annual variations observed over the period 1992-1996 from the tide gauges.

Conclusion

The current accuracy of the T/P altimeters enable observations of annual deviations in the main constituent M_2 . This new knowledge about the spatial behaviour of the signal in the North Sea was compared with output from a hydrodynamical model. The barotropic model confirmed that the seasonal variation is a shallow water phenomena, which was previously indicated from investigations based on coastal tide gauge data alone. The non linear interaction between the tides and the surges is seen to be an important factor for the seasonal variation. Despite the relatively poor spatial resolution of the model, the main part of the seasonal variation is still seen as a barotropic phenomenon. Future investigations with a model on a finer grid would include more of the very near coastal shoaling effects, and give a more precise estimate of the magnitude of the barotropic effects, and indicate the possible existence of baroclinic effects of the seasonal variation in M_2 .

Acknowledgments. This work is a contribution to the GEOSONAR project under the Danish Earth Observation Programme supported by the Danish Research Councils. The authors wish to thank the NASA Altimeter Pathfinder project, the British, French, Belgium, German and Danish hydrographic data providers for data, R. A. Flather, J. A. Williams and P. L. Woodworth, POL, UK for kindly providing model data and for valuable discussions.

References

- Andersen, O. B., Shallow water tides in the northwest European shelf region from TOPEX/POSEIDON altimetry, *Journal of Geophysical Research*, 104, C4, 7729-7741, 1999.
- Baker, T. F. and G. A. Alcock, Time variations of ocean tides, in *Proc. 9th Int. Symp. Earth Tides*, edited by J. T. Kuo, pp. 341-348, Schweizerbart, Stuttgart, 1983.
- Cartwright, D. E., A unified analysis of tides and surges round north and east Britain, *Phil. Trans. R. Soc., London, A* 263, 1-55, 1968.
- Cartwright, D. E. and R. J. Taylor, New computations of the tide-generating potential, *Geophys. J. R. Astron. Soc.*, 23, 45-74, 1971.
- Corkan, R. H., An annual perturbation in the range of tide, *Proc. R. Soc. London, A* 144, 537-559, 1934.

- Flather, R. A., A tidal model of the north-west European continental shelf, *Mémoires Société Royale des Sciences de Liège, 6^e série, tome X*, 141-164, 1976.
- Pugh, D. T. and J. M. Vassie, Tide and Surge Propagation Off-shore in the Dowsing Region of the North Sea, *Deutsche Hydrographische Zeitschrift*, 29, 5, 163-213, 1976.
- Pugh, D. T. and J. M. Vassie, Seasonal Modulations of the Principal Semidiurnal Lunar Tide, in *Mixing and Transport in the Environment*, edited by K. J. Beven, P. C. Chatwin and J. H. Milbank, 247-267, John Wiley & Sons Ltd., 1994.
- Reistad, M. and K. Iden, Updating, correction and evaluation of a hindcast data base of air pressure, wind and waves for the North Sea, the Norwegian Sea and the Barents Sea, *Research Report No. 9*, Norwegian Meteorological Institute, Oslo, Norway, 1998.
- Woodworth, P. L., S. M. Shaw and D. L. Blackman, Secular trends in the mean tidal range around the British Isles and along the adjacent European coastline, *Geophys. J. Int.*, 104, 593-609, 1991.

V. Huess, Danish Meteorological Institute, Lyngbyvej 100, DK-2100 Copenhagen, Denmark. (email: vh@dmi.dk)

O. B. Andersen, National Survey and Cadastre, Rentemestervej 8, DK-2400 Copenhagen, Denmark. (email: oa@kms.dk)

Received June 20, 2000; accepted November 27, 2000.

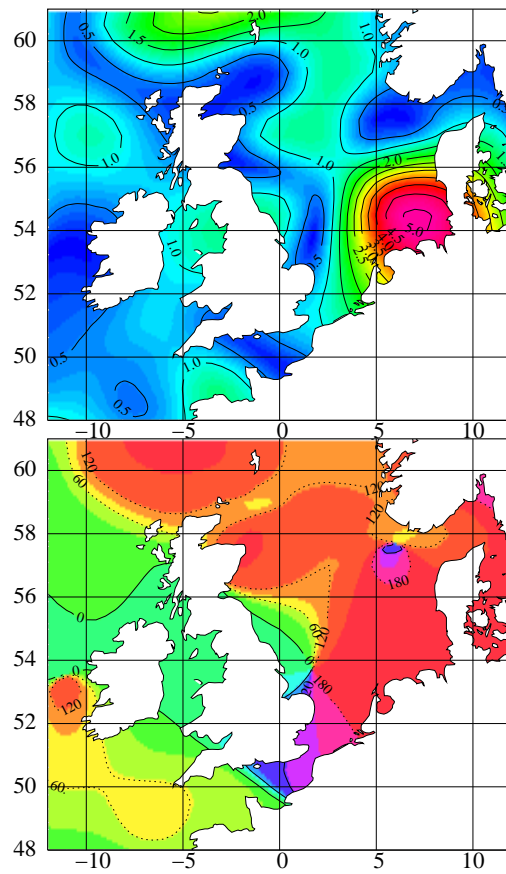


Figure F.3: Plate 1: Maximum deviations in the M_2 constituent from T/P data. Maximum amplitude [cm] (top) and phase lag [deg.] (bottom).

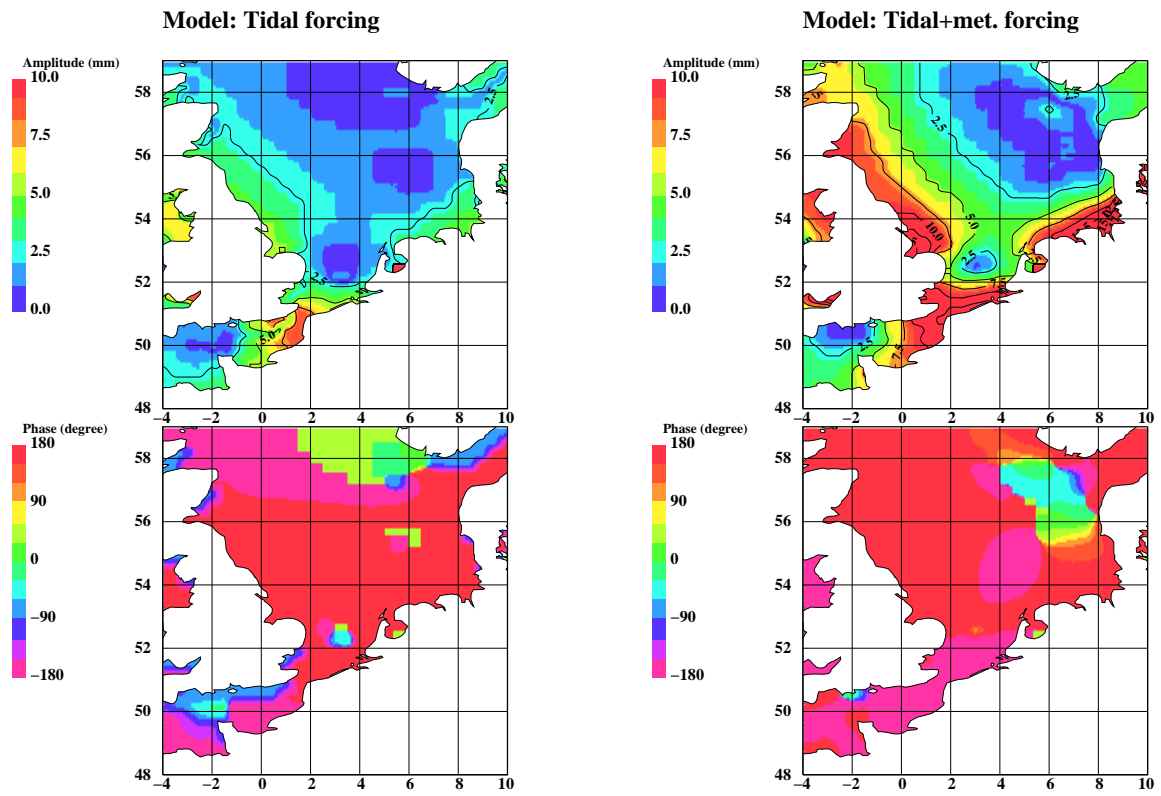


Figure F.4: Plate 2: Model simulated M_2 modulation wave for 1992. Maximum amplitude [cm] (top) and phase lags (bottom). Results from a tidal run (left) and a tidal+met. run (right).

DANISH METEOROLOGICAL INSTITUTE

Scientific Reports

Scientific reports from the Danish Meteorological Institute cover a variety of geophysical fields, i.e. meteorology (including climatology), oceanography, subjects on air and sea pollution, geomagnetism, solar-terrestrial physics, and physics of the middle and upper atmosphere.

Reports in the series within the last five years:

No. 96-1

Poul Frich (co-ordinator), H. Alexandersson, J. Ashcroft, B. Dahlström, G.R. Demarée, A. Drebs, A.F.V. van Engelen, E.J. Førland, I. Hanssen-Bauer, R. Heino, T. Jónsson, K. Jonasson, L. Keegan, P.Ø. Nordli, **T. Schmith, P. Steffensen**, H. Tuomenvirta, O.E. Tveito: North Atlantic Climatological Dataset (NACD Version 1) - Final report

No. 96-2

Georg Kjærgaard Andreasen: Daily response of high-latitude current systems to solar wind variations: application of robust multiple regression. Methods on Godhavn magnetometer data

No. 96-3

Jacob Woge Nielsen, Karsten Bolding Kristensen, Lonny Hansen: Extreme sea level highs: a statistical tide gauge data study

No. 96-4

Jens Hesselbjerg Christensen, Ole Bøssing Christensen, Philippe Lopez, Erik van Meijgaard, Michael Botzet: The HIRLAM4 Regional Atmospheric Climate Model

No. 96-5

Xiang-Yu Huang: Horizontal diffusion and filtering in a mesoscale numerical weather prediction model

No. 96-6

Henrik Svensmark and Eigil Friis-Christensen: Variation of cosmic ray flux and global cloud coverage - a missing link in solar-climate relationships

No. 96-7

Jens Havskov Sørensen and Christian Ødum Jensen: A computer system for the management of epidemiological data and prediction of risk and economic consequences during outbreaks of foot-and-mouth disease. CEC AIR Programme. Contract No. AIR3 - CT92-0652

No. 96-8

Jens Havskov Sørensen: Quasi-automatic of input for LINCOM and RIMPUFF, and output conversion. CEC AIR Programme. Contract No. AIR3 - CT92-0652

No. 96-9

Rashpal S. Gill and Hans H. Valeur: Evaluation of the radarsat imagery for the operational mapping of sea ice around Greenland

No. 96-10

Jens Hesselbjerg Christensen, Bennert Machenhauer, Richard G. Jones, Christoph Schär, Paolo Michele Ruti, Manuel Castro and Guido Visconti: Validation of present-day regional climate simulations over Europe: LAM simulations with observed boundary conditions

No. 96-11

Niels Larsen, Bjørn Knudsen, Paul Eriksen, Ib Steen Mikkelsen, Signe Bech Andersen and Torben Stockflet Jørgensen: European Stratospheric Monitoring Stations in the Arctic: An European contribution to the Network for Detection of Stratospheric Change (NDSC): CEC Environment Programme Contract EV5V-CT93-0333: DMI contribution to the final report

No. 96-12

Niels Larsen: Effects of heterogeneous chemistry on the composition of the stratosphere: CEC Environment Programme Contract EV5V-CT93-0349: DMI contribution to the final report

No. 97-1

E. Friis Christensen og C. Skøtt: Contributions from the International Science Team. The Ørsted Mission - a pre-launch compendium

No. 97-2

Alix Rasmussen, Sissi Kiilsholm, Jens Havskov Sørensen, Ib Steen Mikkelsen: Analysis of tropospheric ozone measurements in Greenland: Contract No. EV5V-CT93-0318 (DG 12 DTEE): DMI's contribution to CEC Final Report Arctic Tropospheric Ozone Chemistry ARCTOC

No. 97-3

Peter Thejll: A search for effects of external events on terrestrial atmospheric pressure: cosmic rays

No. 97-4

Peter Thejll: A search for effects of external events on terrestrial atmospheric pressure: sector boundary crossings

No. 97-5

Knud Lassen: Twentieth century retreat of sea-ice in the Greenland Sea

No. 98-1

Niels Woetman Nielsen, Bjarne Amstrup, Jess U. Jørgensen:

HIRLAM 2.5 parallel tests at DMI: sensitivity to type of schemes for turbulence, moist processes and advection

No. 98-2

Per Høeg, Georg Bergeton Larsen, Hans-Henrik Benzon, Stig Syndergaard, Mette Dahl Mortensen: The GPSOS project

Algorithm functional design and analysis of ionosphere, stratosphere and troposphere observations

No. 98-3

Mette Dahl Mortensen, Per Høeg:

Satellite atmosphere profiling retrieval in a nonlinear troposphere

Previously entitled: Limitations induced by Multipath

No. 98-4

Mette Dahl Mortensen, Per Høeg:

Resolution properties in atmospheric profiling with GPS

No. 98-5

R.S. Gill and M. K. Rosengren

Evaluation of the Radarsat imagery for the operational mapping of sea ice around Greenland in 1997

No. 98-6

R.S. Gill, H.H. Valeur, P. Nielsen and K.Q. Hansen: Using ERS SAR images in the operational mapping of sea ice in the Greenland waters: final report for ESA-ESRIN's: pilot projekt no. PP2.PP2.DK2 and 2nd announcement of opportunity for the exploitation of ERS data projekt No. AO2..DK 102

No. 98-7

Per Høeg et al.: GPS Atmosphere profiling methods and error assessments

No. 98-8

H. Svensmark, N. Woetmann Nielsen and A.M. Sempreviva: Large scale soft and hard turbulent states of the atmosphere

No. 98-9

Philippe Lopez, Eigil Kaas and Annette Guldborg: The full particle-in-cell advection scheme in spherical geometry

No. 98-10

H. Svensmark: Influence of cosmic rays on earth's climate

No. 98-11

Peter Thejll and Henrik Svensmark: Notes on the method of normalized multivariate regression

No. 98-12

K. Lassen: Extent of sea ice in the Greenland Sea 1877-1997: an extension of DMI Scientific Report 97-5

No. 98-13

Niels Larsen, Alberto Adriani and Guido DiDonfrancesco: Microphysical analysis of polar stratospheric clouds observed by lidar at McMurdo, Antarctica

No.98-14

Mette Dahl Mortensen: The back-propagation method for inversion of radio occultation data

No. 98-15

Xiang-Yu Huang: Variational analysis using spatial filters

No. 99-1

Henrik Feddersen: Project on prediction of climate variations on seasonal to interannual time-scales (PROVOST) EU contract ENVA4-CT95-0109: DMI contribution to the final report: Statistical analysis and post-processing of uncoupled PROVOST simulations

No. 99-2

Wilhelm May: A time-slice experiment with the ECHAM4 A-GCM at high resolution: the experimental design and the assessment of climate change as compared to a greenhouse gas experiment with ECHAM4/OPYC at low resolution

No. 99-3

Niels Larsen et al.: European stratospheric monitoring stations in the Arctic II: CEC Environment and Climate Programme Contract ENV4-CT95-0136. DMI Contributions to the project

- No. 99-4
Alexander Baklanov: Parameterisation of the deposition processes and radioactive decay: a review and some preliminary results with the DERMA model
- No. 99-5
Mette Dahl Mortensen: Non-linear high resolution inversion of radio occultation data
- No. 99-6
Stig Syndergaard: Retrieval analysis and methodologies in atmospheric limb sounding using the GNSS radio occultation technique
- No. 99-7
Jun She, Jacob Woge Nielsen: Operational wave forecasts over the Baltic and North Sea
- No. 99-8
Henrik Feddersen: Monthly temperature forecasts for Denmark - statistical or dynamical?
- No. 99-9
P. Thejll, K. Lassen: Solar forcing of the Northern hemisphere air temperature: new data
- No. 99-10
Torben Stockflet Jørgensen, Aksel Walløe Hansen: Comment on "Variation of cosmic ray flux and global coverage - a missing link in solar-climate relationships" by Henrik Svensmark and Eigil Friis-Christensen
- No. 99-11
Mette Dahl Meincke: Inversion methods for atmospheric profiling with GPS occultations
- No. 99-12
Hans-Henrik Benzon; Laust Olsen; Per Høeg: Simulations of current density measurements with a Faraday Current Meter and a magnetometer
- No. 00-01
Per Høeg; G. Leppelmeier: ACE - Atmosphere Climate Experiment
- No. 00-02
Per Høeg: FACE-IT: Field-Aligned Current Experiment in the Ionosphere and Thermosphere
- No. 00-03
Allan Gross: Surface ozone and tropospheric chemistry with applications to regional air quality modeling. PhD thesis
- No. 00-04
Henrik Vedel: Conversion of WGS84 geometric heights to NWP model HIRLAM geopotential heights
- No. 00-05
Jérôme Chenevez: Advection experiments with DMI-Hirlam-Tracer
- No. 00-06
Niels Larsen: Polar stratospheric clouds micro-physical and optical models
- No. 00-07
Alix Rasmussen: "Uncertainty of meteorological parameters from DMI-HIRLAM"
- No. 00-08
A.L. Morozova: Solar activity and Earth's weather. Effect of the forced atmospheric transparency changes on the troposphere temperature profile studied with atmospheric models
- No. 00-09
Niels Larsen, Bjørn M. Knudsen, Michael Gauss, Giovanni Pitari: Effects from high-speed civil traffic aircraft emissions on polar stratospheric clouds
- No. 00-10
Søren Andersen: Evaluation of SSM/I sea ice algorithms for use in the SAF on ocean and sea ice, July 2000
- No. 00-11
Claus Petersen, Niels Woetmann Nielsen: Diagnosis of visibility in DMI-HIRLAM
- No. 00-12
Erik Buch: A monograph on the physical oceanography of the Greenland waters
- No. 00-13
M. Steffensen: Stability indices as indicators of lightning and thunder
- No. 00-14
Bjarne Amstrup, Kristian S. Mogensen, Xiang-Yu Huang: Use of GPS observations in an optimum interpolation based data assimilation system
- No. 00-15
Mads Hvid Nielsen: Dynamisk beskrivelse og hydrografisk klassifikation af den jyske kyststrøm

No. 00-16

Kristian S. Mogensen, Jess U. Jørgensen, Bjarne Amstrup, Xiaohua Yang and Xiang-Yu Huang: Towards an operational implementation of HIRLAM 3D-VAR at DMI

No. 00-17

Sattler, Kai; Huang, Xiang-Yu: Structure function characteristics for 2 meter temperature and relative humidity in different horizontal resolutions

No. 00-18

Niels Larsen, Ib Steen Mikkelsen, Bjørn M. Knudsen m.fl.: In-situ analysis of aerosols and gases in the polar stratosphere. A contribution to THESEO. Environment and climate research programme. Contract no. ENV4-CT97-0523. Final report

No. 00-19

Amstrup, Bjarne: EUCOS observing system experiments with the DMI HIRLAM optimum interpolation analysis and forecasting system

No. 01-01

V.O. Papitashvili, L.I. Gromova, V.A. Popov and O. Rasmussen: Northern polar cap magnetic activity index PCN: Effective area, universal time, seasonal, and solar cycle variations

No. 01-02

M.E. Gorbunov: Radiological methods for processing radio occultation data in multipath regions

No. 01-03

Niels Woetmann Nielsen; Claus Petersen: Calculation of wind gusts in DMI-HIRLAM

No. 01-04

Vladimir Penenko; Alexander Baklanov: Methods of sensitivity theory and inverse modeling for estimation of source parameter and risk/vulnerability areas

No. 01-05

Sergej Zilitinkevich; Alexander Baklanov; Jutta Rost; Ann-Sofi Smedman, Vasiliy Lykosov and Pierluigi Calanca: Diagnostic and prognostic equations for the depth of the stably stratified Ekman boundary layer

No. 01-06

Bjarne Amstrup: Impact of ATOVS AMSU-A radiance data in the DMI-HIRLAM 3D-Var analysis and forecasting system

No. 01-07

Sergej Zilitinkevich and Alexander Baklanov: Calculation of the height of stable boundary layers in operational models.

No. 01-08

Vibeke Huess: Sea level variations in the North Sea - from tide gauges, altimetry and modelling.